Cell Reports

Resource

# Parallel genetics of regulatory sequences using scalable genome editing *in vivo*

## Graphical abstract

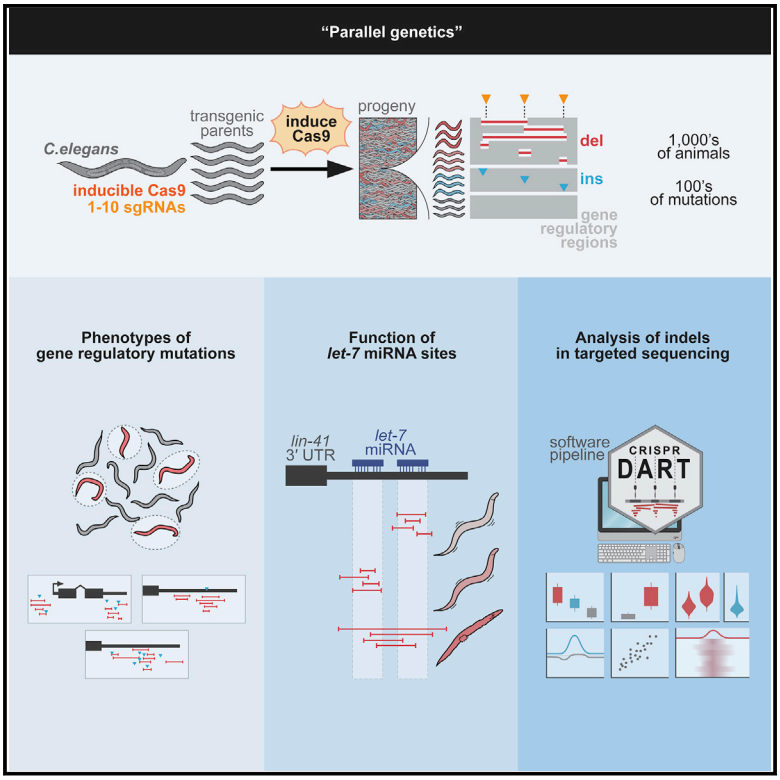


## Authors

Jonathan J. Froehlich, Bora Uyar, Margareta Herzog, Kathrin Theil, Petar Glažar, Altuna Akalin, Nikolaus Rajewsky

## Correspondence

rajewsky@mdc-berlin.de

## In brief

Animal phenotypes rely on gene-regulatory mechanisms. Froehlich et al. develop parallel genome editing in *C. elegans* to produce diverse indel mutations at regulatory DNA. They describe indel characteristics, study the function of two adjacent microRNA binding sites, and directly map gene-regulatory genotypes to animal phenotypes.

## Highlights

- Inducible Cas9 in *C. elegans* populations produces targeted indels in parallel
- "crispr-DART" software to analyze indel mutations in targeted DNA sequencing
- Two *let-7* miRNA binding sites in the *lin-41* 3′ UTR can function independently
- Gene-regulatory mutations are mapped to morphological phenotypes

Froehlich et al., 2021, Cell Reports *35*, 108988
April 13, 2021 
https://doi.org/10.1016/j.celrep.2021.108988

CellPress

Cell Reports

CellPress
OPEN ACCESS

Resource

# Parallel genetics of regulatory sequences using scalable genome editing *in vivo*

Jonathan J. Froehlich,[1,3] Bora Uyar,[2,3] Margareta Herzog,[1] Kathrin Theil,[1] Petar Glažar,[1] Altuna Akalin,[2] and Nikolaus Rajewsky[1,4,*]

[1]Systems Biology of Gene Regulatory Elements, Berlin Institute for Medical Systems Biology, Max Delbrück Center for Molecular Medicine in the Helmholtz Association, Hannoversche Str. 28, 10115 Berlin, Germany

[2]Bioinformatics and Omics Data Science Platform, Berlin Institute for Medical Systems Biology, Max Delbrück Center for Molecular Medicine in the Helmholtz Association, Hannoversche Str. 28, 10115 Berlin, Germany

[3]These authors contributed equally

[4]Lead contact

*Correspondence: rajewsky@mdc-berlin.de

https://doi.org/10.1016/j.celrep.2021.108988

## SUMMARY

How regulatory sequences control gene expression is fundamental for explaining phenotypes in health and disease. Regulatory elements must ultimately be understood within their genomic environment and development- or tissue-specific contexts. Because this is technically challenging, few regulatory elements have been characterized *in vivo*. Here, we use inducible Cas9 and multiplexed guide RNAs to create hundreds of mutations in enhancers/promoters and 3′ UTRs of 16 genes in *C. elegans*. Our software crispr-DART analyzes indel mutations in targeted DNA sequencing. We quantify the impact of mutations on expression and fitness by targeted RNA sequencing and DNA sampling. When applying our approach to the *lin-41* 3′ UTR, generating hundreds of mutants, we find that the two adjacent binding sites for the miRNA *let-7* can regulate *lin-41* expression independently of each other. Finally, we map regulatory genotypes to phenotypic traits for several genes. Our approach enables parallel analysis of regulatory sequences directly in animals.

## INTRODUCTION

Understanding gene regulation is fundamental for understanding development and tissue function in health and disease. Animal genomes contain diverse regulatory sequences that are organized in contiguous stretches of genomic DNA, ranging from a few to hundreds or thousands of bases. Promoters, enhancers, and silencers act mainly on transcription, whereas mRNA 5′ and 3′ untranslated regions (UTRs) mainly regulate mRNA export, localization, degradation, and translation. Many gene-regulatory sequences encode multiple functions that can cooperate, compensate, and compete (Davidson, 2010; Levo and Segal, 2014; Long et al., 2016). Understanding this logic requires combinatorial perturbations. Moreover, a single binding site, because of fuzzy recognition motifs, may tolerate certain mutations (Chen and Rajewsky, 2007; Farley et al., 2015; Jankowsky and Harris, 2015). The interaction between effectors and regulatory elements can be modulated by sequence structure, co-factors, chemical modifications, and the temporal order of binding, and sequence activity is dependent on native sequence context, cell type, development, and the environment (Davidson, 2010; Dominguez et al., 2018; Jankowsky and Harris, 2015; Levo and Segal, 2014; Long et al., 2016). Mechanisms that confer robustness or stochasticity of phenotype add another layer of complexity to this (Burga and Lehner, 2012; Kontarakis and Stainier, 2020; Macneil and Walhout, 2011; Smits et al., 2019). Accordingly, phenotypic consequences of gene-regulatory mutations are difficult to predict. To understand biological functions and mechanisms in animals, scalable approaches to target regulatory sequences with many different mutations are required.

Although massively parallel functional assays of regulatory sequences have been developed in cell lines and yeast (Canver et al., 2015; Findlay et al., 2014; Gasperini et al., 2016; Shendure and Fields, 2016; Vierstra et al., 2015), few *in vivo* approaches have been achieved in animal models. These use integration of reporters (Fuqua et al., 2020; Kvon et al., 2020) or injection of RNA libraries (Rabani et al., 2017; Yartseva et al., 2017) and, therefore, do not evaluate endogenous phenotypes or are restricted to one stage of the animal life cycle. Classical genome editing by injection, now widely accessible because of CRISPR-Cas-based techniques, has enabled functional tests, but this is still labor intensive and limited in scalability (Anzalone et al., 2020; Barrangou and Doudna, 2016; Hörnblad et al., 2021; Labi et al., 2019).

Here, we use inducible expression of Cas9 and multiplexed single guide RNAs in *Caenorhabditis elegans* populations to generate hundreds of targeted mutations in parallel. We targeted different regulatory regions across 16 genes and analyzed more than 12,000 Cas9-induced mutations to first describe characteristics of double-stranded DNA (dsDNA) break repair in the

*C. elegans* germline and the introduced genotype diversity at the targeted loci. We then applied our mutagenesis approach to generate hundreds of deletions along the well-studied *lin-41* 3′ UTR, which is targeted by the microRNA (miRNA) *let-7* (Ecsedi et al., 2015; Reinhart et al., 2000; Vella et al., 2004a). We developed an RNA sequencing-based strategy to quantify the effect of each mutation on *lin-41* RNA level. Using DNA sequencing, we followed the relative abundance of these different mutations over several generations to infer their phenotype. Finally, we couple the targeted mutagenesis of regulatory sequences to selection by phenotypic traits. We isolate 57 alleles in 3 genes that show strong morphological defects in phenotype, mediated by mutations in an enhancer, TATA box, and 3′ UTRs.

## RESULTS

### Cas9 induction for targeted and parallel mutagenesis in *C. elegans* populations

To introduce many different targeted mutations *in vivo*, we developed a scalable approach in *C. elegans* using inducible expression of Cas9 and several multiplexed single guide RNAs (sgRNAs). This required only a few initial injections to create transgenic animals, allowed maintenance without mutagenesis, and enabled time-controlled creation of mutated populations in parallel, with sizes only limited by culturing approaches (up to $\sim 10^6$ in our case). Mutant populations could then be used for various purposes. For example, they could be selected by phenotype or reporter activity or analyzed directly by targeted sequencing to measure the effect of mutations on RNA levels or fitness (Figure 1A).

As an initial test, we generated transgenic lines with plasmids for heat shock-driven Cas9 expression and one or multiple sgRNAs targeting a ubiquitously expressed single-copy GFP reporter. After a transient heat shock, we could observe GFP-negative animals in culture, indicating activity of Cas9. We performed a 2-h heat shock induction of Cas9 in the parents (P0) and collected progeny (F1) in a time course experiment. The highest fractions of mutants were obtained 14–16 h after heat shock, with approximately 50% (sg1) and 20% (sg2) of eggs producing GFP-negative animals (Figure S1A). We obtained similar results when we targeted the *dpy-10* gene and counted the characteristic Dumpy (Dpy) phenotype, comparing two plasmids for heat shock-induced expression of Cas9. Eggs collected 12–15 h after heat shock produced around 20%–35% of Dpy animals with both plasmids (Figure S1B). We also found that a U6 promoter with a reported higher gonad expression (Diag et al., 2018) resulted in a larger number of Dpy progeny on average (Figure S1C).

Characteristic CRISPR-Cas9-induced mutations from 91 GFP-negative animals consisted of insertions or deletions (indels) or a combination of both and originated from sgRNA cut sites (Figures S1D and S1E). When we used three sgRNAs within the same transgenic line, targeting adjacent positions, deletions appeared around one cut site or spanned two cut sites (Figure S1E). This indicated that pools of sgRNAs could lead to more diverse genotypes and cover more nucleotides. Most deletions induced by a single sgRNA were between 3–10 bp long, and we observed insertion lengths between 1–30 bp (Figure S1F).

Homozygous animals would be produced in the F2 by heterozygous self-fertilizing F1. Additionally, if Cas9 induced in P0 would still be active after fertilization, F1 animals could be mosaic with a wild-type germline and mutant somatic cells (Figure S1G). We therefore wanted to assess how many germline mutations were generated in the F1. For this, we analyzed the inheritance of the GFP-negative phenotype from F1 to F2 generations using an automated flow system and found that ~80% of mutations were indeed germline mutations (Figures S1H–S1J). For the rest of our work, we used such non-mosaic F2, generated by F1 germline mutations.

To analyze large populations of mutated *C. elegans* in bulk, we established a targeted sequencing protocol based on long 0.5- to 3-kb PCR amplicons. This allowed us to sequence the complete targeted locus, place most primers more than 300 bp away from the nearest sgRNA cut site to avoid deletion of primer binding sites, and capture large deletions. Barcoding samples enabled combined sequencing on the same flow cell (Figures S2A–S2C). To handle targeted sequencing data of such amplicons and analyze the contained mutations, we created the software pipeline crispr-DART (CRISPR-Cas downstream analysis and reporting tool; https://github.com/BIMSBbioinfo/crispr_DART). The pipeline extracts and quantifies indels from various targeted sequencing technologies, single or multiple regions of interest, and single- or multiplexed sgRNAs. The output contains reports of coverage, indel mutation profiles, sgRNA efficiencies, and optional comparisons between samples to identify differential regions and mutations. Processed genomics files from the output can be used for more in-depth custom analyses with additional supplied R scripts (Figures S2D and S2E; Data and code availability).

To test our approach at a larger scale, we induced Cas9 in 50,000 P0 animals by heat shock and amplicon sequenced the mutated locus from bulk samples of 400,000 F2 progeny. Deletions per genomic base pair peaked sharply around sgRNA cut sites (Figure 1B). Pools of multiplexed sgRNA plasmids resulted in deletions spanning two or several sgRNAs (multi-cut) in addition to smaller deletions surrounding single sgRNAs (single-cut) (Figure 1B, bottom). Insertions occurred within a few nucleotides to cut sites and were less frequent than deletions (~1/2–1/10$^{th}$; Figure 1C). We observed background mutations of short 1-bp deletions and insertions that were also present with similar abundance in isogenic wild-type controls and occurred independent of sgRNA cut sites. These could have been caused by biological (e.g., DNA modifications, natural mutations) and technical factors (e.g., during or after extraction of genomic DNA, PCR, sequencing errors). Such mutations were absent in genotyping by Sanger sequencing, and we later established computational filters to separate these from CRISPR-Cas9-induced mutations.

### Features of CRISPR-Cas9-induced indels

To understand gene-regulatory logic, ideally, many different variants are produced with high efficiency that can then be tested for their effects *in vivo*. We set out to analyze the efficiency and characteristics of mutations produced with our approach. We targeted 16 genes at different regions with 1–9 sgRNAs per

CellPress
OPEN ACCESS

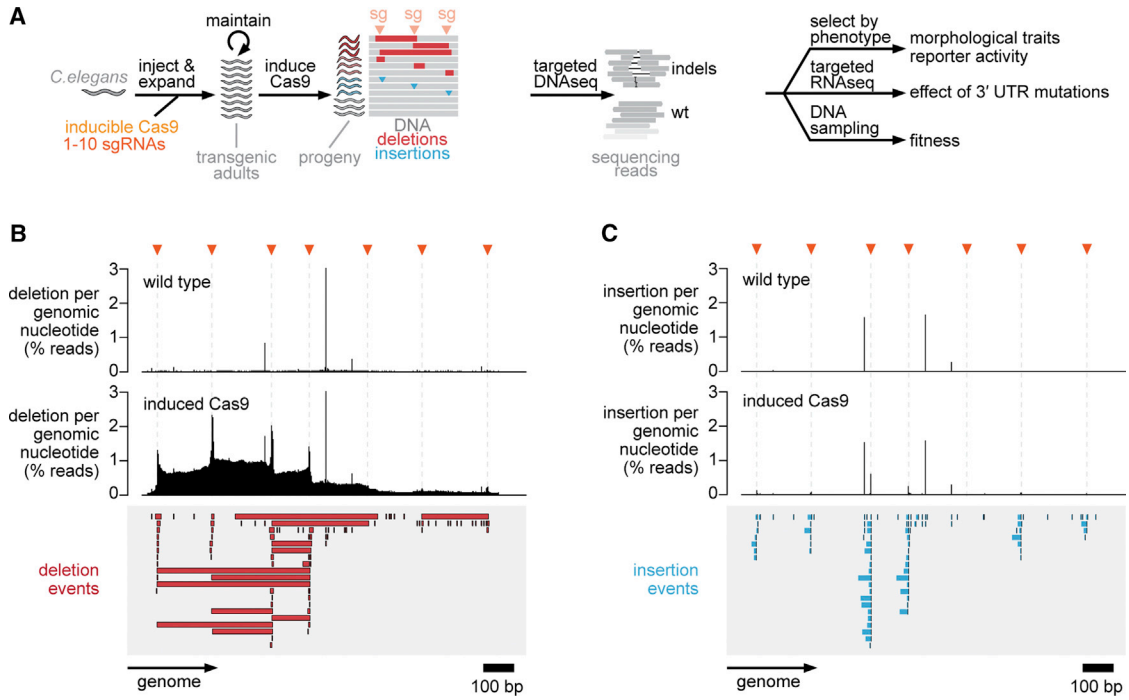


**Figure 1. Cas9 induction for targeted and parallel mutagenesis in *C. elegans* populations**

(A) Outline of our approach. Heat shock Cas9 induction creates large "diversified" populations containing indel mutations at the targeted region. Mutated populations can be used for various downstream assays: selection by morphological traits or reporter activity, bulk RNA sequencing to measure effects of individual 3′ UTR mutations, or DNA sampling over several generations to infer fitness of different genotypes.

(B) Example of the complete spectrum of observed mutations after targeting a locus. The percentage of DNA sequencing reads containing deletions with respect to the total read coverage is plotted at the corresponding genomic position. Bulk worm samples were sequenced; thus, 2% deletions per genomic nucleotide refers to approximately 2% of worms with a deletion at the respective nucleotide. Orange triangles, sgRNA cut sites. Individual deletion events are shown below in red.

(C) Same analysis as in (B) but for insertion events.

See also Figures S1 and S2.

transgenic line. These genes were selected for different downstream experiments and contained one gene with a known miRNA interaction, 8 genes with known reduction-of-function phenotypes, and 7 essential genes. After Cas9 heat shock induction, we sequenced bulk genomic DNA from 400,000 F2 animals with long amplicon sequencing. Together with wild-type controls, this produced data for 60 samples and 91 sgRNAs (Tables S1 and S3).

To measure sgRNA efficiencies, we counted all reads with deletions overlapping ±5 bp of a given sgRNA cut site and normalized this value by the number of total reads at that position. The median efficiency was 1.4%, with most sgRNAs showing efficiencies of 0%–6.3% (95% confidence interval [CI]) (Figure 2A). 1.4% corresponded to approximately 5,600 mutant animals per sgRNA in our samples. We then compared observed sgRNA efficiencies with published efficiency prediction scores but found no significant predictive power (Figure S2F). Possible reasons for this could be that these scores were obtained in other experimental models or that sequence-independent factors were dominating in our system. Also, the injected plasmid concentrations during generation of transgenic lines were not correlated with efficiency (Figure S2G). We found, however, that sgRNAs for target sites with two guanines preceding the protospacer adjacent motif (PAM) were significantly more efficient, as described previously for *C. elegans* ("GGNGG sites"; Farboud and Meyer, 2015; Figure S2H). Also, lethal phenotypes were likely not confounding these analyses (e.g., by depleting for animals with efficient sgRNAs) (Figure S2I). We then used the detected mutations to characterize CRISPR-Cas9-induced dsDNA break repair outcomes in the *C. elegans* germline. We analyzed the proportion of mutation types present in sequencing reads from each sample. On average, samples contained 57.9% deletions, 22.9% insertions, and 19.3% complex events (combinations of insertions, deletions, and substitutions) (Figure 2B). These proportions are similar for naturally occurring germline indels in *C. elegans* (75% deletions, 25% insertions) (Konrad et al., 2019) and human (50% deletions, 35% insertions) (Collins et al., 2020).

The targeted sequencing approach resulted in a uniform read coverage per amplicon between 200,000- to 800,000-fold. We empirically determined general read support thresholds to robustly detect mutations in treated samples while observing few mutations in the isogenic wild-type controls. An indel had to be supported by at least 0.001% reads mapped to a position, at least 5 reads, and overlap with a sgRNA cut site ±5 bp. We excluded complex events (combinations of insertions, deletions, and substitutions) from the rest of our analyses to be more certain about the resulting sequences. 100 ng of genomic DNA was used as input for our sequencing protocol, representing

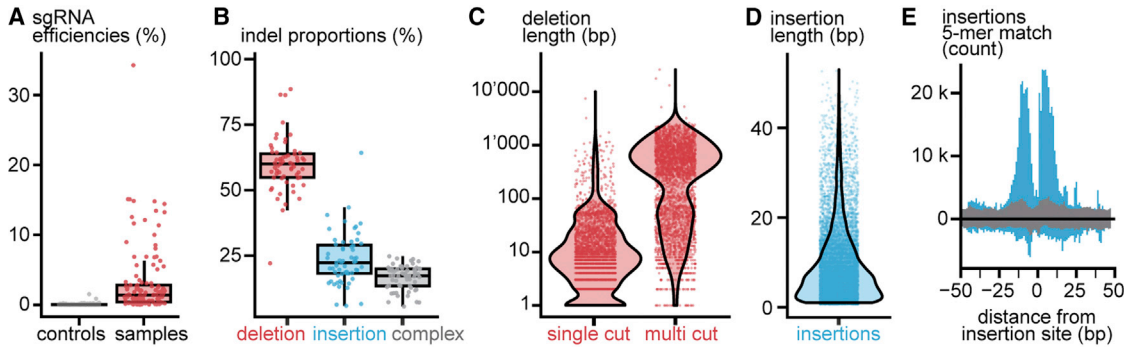


**Figure 2. Features of CRISPR-Cas9-induced indels**

Pooled data from 60 experiments, each sample expressing 1–8 sgRNAs targeting one region among 16 genes (n = 24 wild-type controls, n = 36 samples with induced Cas9).

(A) Efficiency measured for each sgRNA per experiment (n = 127 sgRNAs).

(B) Proportions of reads with different types of mutations detected in each experiment (n = 60 experiments). "Complex" indels, reads with more than one indel or additional adjacent substitutions.

(C) Length distribution of deletions found in all treated samples (n = 2,915 multi-cut and 3,169 single-cut deletions).

(D) Length distribution of insertions found in all experiments (n = 6,616 insertions).

(E) Matches of 5-mers from insertions (blue) to surrounding sequence (±50 bp). Randomly shuffled insertion sequences were used as controls (gray). Data are from 34 samples.

See also Figure S3.

more than 90 million genomes, enough to cover all animals in our samples. With the assumption that animals contributed equally to the extracted genomic DNA, we estimated that 4–10 mutants among 400,000 animals were sufficient to detect a mutation, depending on the amplicon coverage (Figure S3A).

Using these thresholds, we detected 12,700 indels in our samples. We computationally separated deletions into single- or multi-cut based on overlap with cut sites (Figure S3B). The length of single-cut deletions ranged from 1 to over 100 bp, with the majority around 5–25 bp. Because larger deletions have a higher chance of overlapping with a second sgRNA cut site, this is likely an underestimation. Multi-cut deletions were larger, mostly several hundred base pairs, as expected from the spacing between multiplexed sgRNAs (Figure 2C). Most (>90%) insertions were 1–20 bp long, although we could find insertions up to 45 bp (Figure 2D). These length distributions were similar to our observations made by Sanger sequencing (Figure S1E).

Inspection of individual genotypes revealed that most insertions contained short sequences also found in close proximity to the insertion position (Figure S3C and S3D). Using our deep sequencing data, we systematically analyzed such microhomologous matches between insertions and the surrounding regions. 5-mers from insertions matched to sequences in a window ±13 bp around the insertion position and only in the same orientation (Figure 2E; Figures S3E and S3F). Thus, our data indicate that many insertions are duplications of surrounding microhomologous sequences occurring mainly in the same orientation. This could be the result of a dissociation and re-annealing during microhomology-mediated end joining of dsDNA breaks (Figure S3G).

## Genotype diversity produced by indels

Finally, we assessed the genotype diversity generated by indels. We considered each unique indel sequence a genotype, given that they reached the filtering thresholds defined before (0.001% reads, 5 reads, cut site overlap). We started by counting the number of unique deletions per base pair. We first studied deletions created by single-cut events for each sgRNA and found that highly active sgRNAs could generate up to 150 unique deletion genotypes and the highest diversity close to cut sites (rows in Figure 3A). Most of these genotypes defined by deletions covered a 10- to 12-bp region surrounding the cut sites. On average, every sgRNA could generate around 15 different genotypes per base pair at the center of the cut site and up to 5 different genotypes per base pair 5 bp away from the cut site (black line profile in Figure 3A). We then studied multi-cut events. Here, we found up to 200 unique deletion genotypes per base pair and, on average, around 20 per sgRNA covering a region more than 500 bp surrounding each cut site (Figure 3B). When counting the number of genotypes generated by one sgRNA, one sgRNA created 50 deletion and 10 insertion genotypes on average. However, some sgRNAs created up to 400 genotypes (Figure 3C). Because we used several sgRNAs per transgenic line, we observed a median of 162 insertion and 190 deletion genotypes per sample and, in the most efficient lines, 1,833 deletion and 1,213 insertion genotypes (Figure 3D). More efficient sgRNAs resulted in a higher number of new genotypes (Figure 3E). Transgenic lines expressing more sgRNAs showed more unique deletion genotypes, possibly because of an increased chance of containing efficient sgRNAs and the combined activity of multiple sgRNAs creating combinatorial deletions (Figure 3F). These data show that inducible expression of Cas9 with multiplexed sgRNAs can induce hundreds of indel-based genotypes in parallel at the targeted regulatory regions. This includes small deletions to target individual regulatory elements at nucleotide resolution, large deletions to interrogate combinatory interactions, and insertions to change the spacing between elements and create semi-random or duplicated sequences.

CellPress
OPEN ACCESS

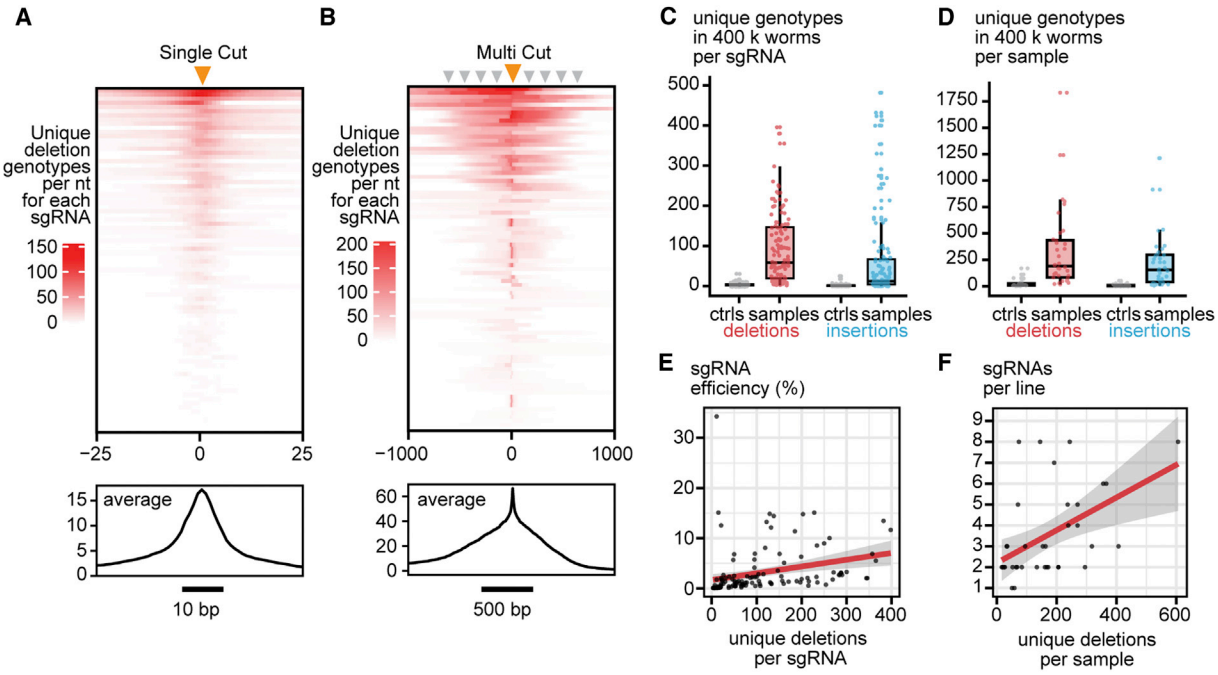


**Figure 3. Genotype diversity produced by indels**

Pooled data from 60 experiments, each sample expressing 1–8 sgRNAs targeting one region among 16 genes (n = 24 wild-type controls (ctrls), n = 36 samples with induced Cas9).

(A and B) Unique deletion genotypes per nucleotide for each sgRNA centered at cut sites. Each row shows the count of distinct genotypes per nucleotide for one sgRNA (n = 86 sgRNAs); black curve on the bottom, average unique deletion genotypes per base pair.

(C) Unique genotypes detected per sgRNA in 400,000 sequenced worms (n = 76 ctrls cut sites, n = 86 samples cut sites) (Wilcoxon, $p < 2.2e{-}16$ for deletions, $p < 2.2e{-}16$ for insertions).

(D) Unique genotypes created per sample by indels (n = 24 ctrls, n = 36 samples) (Wilcoxon, $p = 1.7e{-}08$ for deletions, $p = 4.7e{-}09$ for insertions).

(E) Correlation between sgRNA efficiency and the created unique deletions per sgRNA per sample (n = 91 sgRNAs).

(F) Correlation between the amount of different sgRNAs in a transgenic line and the created unique deletions per sample (n = 6,084 unique deletions, n = 36 treated samples).

## Regulation of *lin-41* mRNA and phenotype by *let-7* miRNA binding sites

A major challenge for understanding gene regulation is the interaction of different elements. Especially in 3′ UTRs, which can act on all levels of gene expression, this can be difficult. To simultaneously measure mRNA levels for all generated 3′ UTR deletions within large *C. elegans* populations, we developed a targeted RNA sequencing strategy. As a proof of principle, we tested it on a miRNA-regulated mRNA. The *lin-41* mRNA is regulated by *let-7* miRNAs that bind two complementary sites in the 1.1-kb-long 3′ UTR (site 1 and site 2, 22 and 20 nt long, respectively, separated by a 27-nt spacer) (Bagga et al., 2005; Ecsedi et al., 2015; Reinhart et al., 2000; Slack et al., 2000; Vella et al., 2004a; Figure S4A). Although studies with reporter plasmids showed that each binding site could not function on its own (Vella et al., 2004a), other studies concluded that each site could recapitulate wild-type regulation when present in three copies (Long et al., 2007). We wanted to explore the function and interaction of the two binding sites in the native sequence context and at natural expression levels. Therefore, we targeted the *lin-41* 3′ UTR with a pool of 8 sgRNAs or, individually, two different pairs of sgRNAs close to the *let-7* binding sites (Figure 4A). *Lin-41* downregulation occurs with *let-7* expression in the larval 3 (L3) and L4 developmental stages (Abbott et al., 2005; Bagga et al., 2005; Reinhart et al., 2000; Slack et al., 2000). To measure *let-7*-dependent regulation, we collected RNA from mutated F2 generation bulk worms at the L1 and L4 stages. We extracted L4-stage RNA after complete *lin-41* mRNA downregulation by *let-7* (Aeschimann et al., 2017) and before occurrence of the lethal vulva-bursting phenotype (Ecsedi et al., 2015; Figure S4B; STAR Methods). We then sequenced *lin-41*-specific cDNA with long reads to cover the complete 3′ UTR (Figure S4C). Each read contained full information about any deletion in the RNA molecule, whereas the number of reads supporting each deletion could be used to estimate RNA expression level. To determine *let-7*-dependent effects, we then analyzed how different deletions affected RNA abundance at the L4- relative to the L1 stage.

We observed an average of more than 4-fold upregulation of *lin-41* mRNA at the L4 stage, when both *let-7* miRNA seed sites were affected by deletions (Figure 4B). A 4-fold regulatory effect is consistent with the known magnitude of downregulation in the natural context (Bagga et al., 2005; Slack et al., 2000; Vella et al., 2004a) or upregulation when disrupting both *let-7* interactions (2- to 4-fold) (Brancati and Großhans, 2018; Ecsedi et al., 2015;

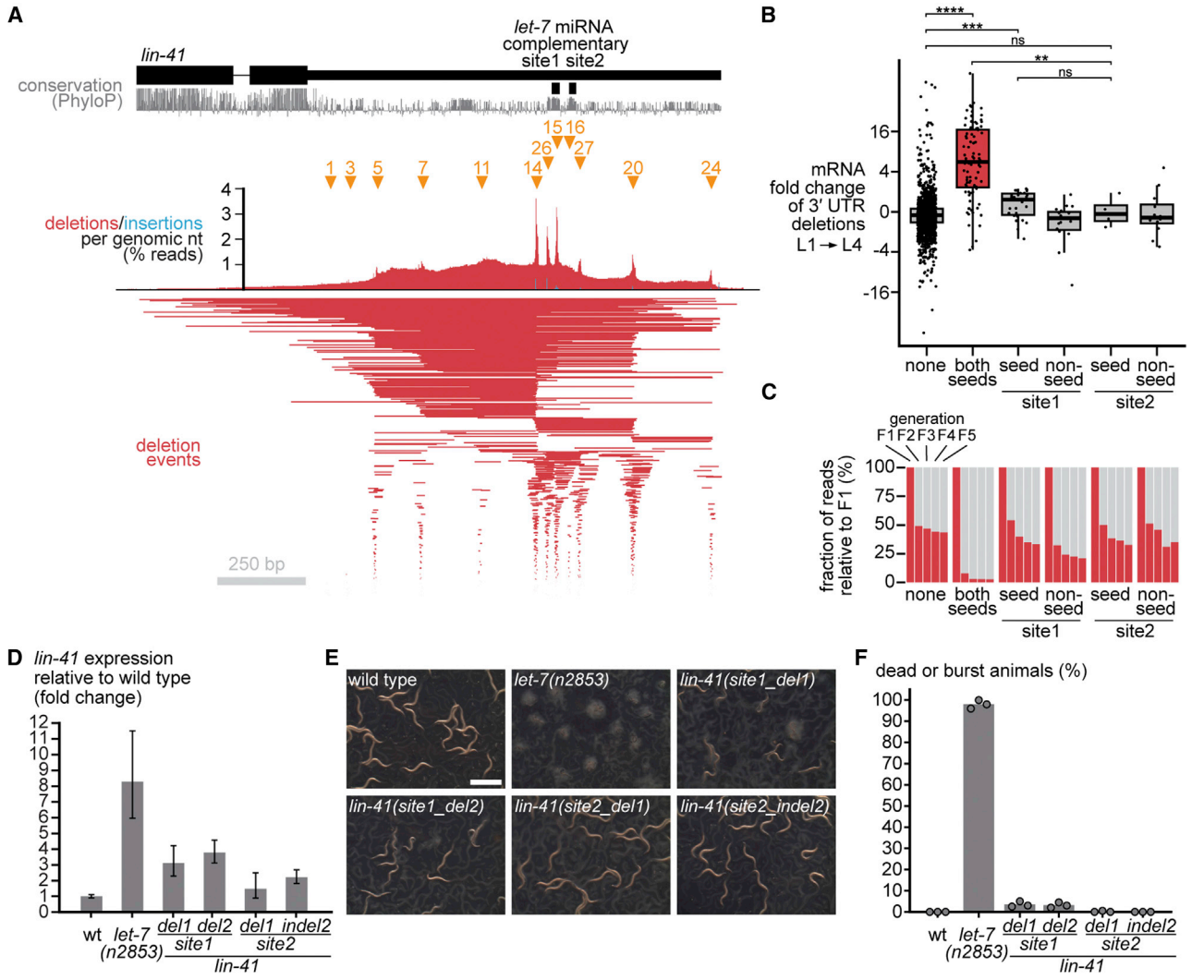


**Figure 4. Regulation of *lin-41* mRNA and phenotype by *let-7* miRNA binding sites**

(A) The *lin-41* 3′ UTR locus after targeted mutagenesis with three different lines (sg pool, sg15+sg16, and sg26+sg27; sgRNA cut sites are indicated by orange triangles). Deletions of three lines were pooled and analyzed together (n > 900 deletion events).

(B) Relative fold change of deletions detected in targeted full-length sequencing of cDNA between the L1 and L4 developmental stages. Deletions are classified by their unique overlap with regions of interest. Non-seed, all nucleotides of the *let-7* complementary sites, excluding the miRNA seed region (see Figure S4A for a detailed diagram) (Wilcoxon rank-sum test; not significant [ns], $p > 0.05$; **$p < 0.01$; ***$p < 0.001$; ****$p < 0.0001$).

(C) Fraction of reads supporting deletions in bulk genomic DNA of consecutive generations relative to the first (F1) generation. Deletions from six samples were pooled for this analysis (sg pool, sg15+sg16, and sg26+sg27, grown at 16°C and 24°C).

(D) *lin-41* mRNA levels in the *let-7* mutant allele *let-7(n2853)* and in *lin-41* strains with deletions affecting site 1 or site 2 relative to wild-type levels, quantified by qPCR. One experiment with 7,000 animals, 30 h into synchronized development at 24°C. Bars represent mean and error bars ± standard deviation.

(E) Phenotype of *lin-41* site 1 and site 2 mutant strains compared with wild-type and *let-7(n2853)*, 50 h into synchronized development at 24°C. Scale, 1 mm.

(F) Dead or burst animals 50 h into synchronized development at 24°C from three plates (n = 3), scoring 200 animals on each plate.

See also Figure S4.

Hunter et al., 2013). Weak but significant upregulation was observed for deletions overlapping with the site 1 seed. We obtained fewer deletions for the site 2 seed and, therefore, did not have the statistical power to rule out a similar weak effect. As an independent approach and to measure the effect of genotypes with multiple deletions per animal, we used unsupervised clustering of long cDNA reads using the k-mer content of reads to obtain clusters representing similar genotypes. These data also suggest that RNA molecules transcribed from genotypes with deletions overlapping both sites were detected with more reads in L4-stage compared with L1-stage animals (see clusters 1–4, 7–8, and 11–13 in Figures S4D–S4F). Additionally, this analysis revealed two other areas that affected mRNA in the opposite way by increasing levels at the L1 stage or decreasing levels at the L4 stage, which could be investigated further in the future (see clusters 5 and 10 in Figure S4F).

To assign fitness to individual mutations in a controlled environment, we established measurements on genotype abundance over several generations. For this, we sampled genomic DNA of consecutive generations. Disrupting *let-7* regulation of *lin-41* mRNA is known to result in lethal developmental defects (Brancati and Großhans, 2018; Ecsedi et al., 2015; Reinhart et al., 2000; Slack et al., 2000; Zhang et al., 2015). We performed this analysis starting at the F1 generation because mosaic animals would be expected to show a phenotype with a fitness disadvantage. Deletions in the *lin-41* 3′ UTR, which overlapped both seeds, disappeared quickly from the population after one generation (Figures 4C and S4G). Consistent with the effect on RNA expression, deletions of both seeds were depleted strongly, whereas deletions affecting either one of the two sites alone were depleted only slightly compared with control deletions not overlapping any features (“none”). This also indicated that deletions with stronger effects were possibly already missing in the mRNA analysis we performed in the F2 generation.

Although deletion of both *let-7* binding sites has been reported to be lethal (Ecsedi et al., 2015), our results showed that deletions of one site could be tolerated. We therefore created two lines for each site with seed-disrupting deletions (Figure S4H). We then compared *lin-41* mRNA expression and phenotypes of homozygous mutants with wild-type animals. To disrupt both *let-7* interactions simultaneously, we used the temperature-sensitive *let-7(n2853)* allele. At the L4 developmental stage, *lin-41* mRNA was upregulated around 8-fold in *let-7(n2853)*, around 3-fold in site 1 mutants, and around 1.5-fold in site 2 mutants (Figure 4D). This could indicate that our high-throughput bulk mRNA measurements were biased toward deletions with smaller effects, possibly because of depletion of animals in the F1 generation. At 50 h into synchronized, we quantified the lethal phenotype that occurs by bursting when *lin-41* regulation by *let-7* is disrupted. Adult animals with mutations in site 2 displayed a normal wild-type phenotype, whereas site 1 mutants were visibly sick but laying eggs. *Let-7* mutants were dead (Figure 4E). We found that, although 98% of *let-7* mutants were dead or had burst, only 3% of site 1 and none of the site 2 mutants showed this phenotype (Figure 4F).

Our results indicate that each of the two *let-7* miRNA binding sites can function on its own and that disruption of site 1 has a stronger effect than disruption of site 2. Furthermore, sites might be able to compensate for each other’s loss to some degree because the effect of disrupting each site alone was weaker than that of combined loss of both sites. We conclude that parallel mutagenesis coupled with targeted RNA or DNA sequencing can be used to directly analyze the function and interactions of regulatory elements *in vivo* from large populations in bulk.

### Screening for functional regulatory sequences that change the morphological phenotype

Next, we wanted to directly map regulatory sequence variants to phenotypic traits. This could be useful to discover functional elements, provide starting points to study regulatory mechanisms, and to explore phenotypic plasticity in animals. Such an approach would also capture any functional sequences regardless of the type, time, or place of regulation. We targeted a predicted enhancer (Jänes et al., 2018), three promoters, and all 3′ UTRs of 8 genes and manually screened 35,000 animals for each of these regions (Table S1). Loss of function and reduction of function of the screened genes are known to result in strong organismal defects in animal movement and body shape (Unc, Slu, Rol, and Dpy). We selected worms based on these phenotypes and identified the causative mutations. Although we screened for general defects in movement and body shape, our approach was biased toward finding reduction- and loss-of-function mutations. To determine which mutations were initially present in the screened population, we performed targeted sequencing on siblings (Figures 5A and S5A). Initially, we isolated several mutants with large deletions (>500 bp) that disrupted the coding sequence or the polyadenylation signal (AATAAA) (Figures S5B and S5C). Similar large-scale, on-target deletions have also been described in cell lines and mice (Adikusuma et al., 2018; Gasperini et al., 2017; Kosicki et al., 2018). We also found large insertions (up to 250 bp) that originated from within ±1 kb of the targeted region or from loci on other chromosomes (Figures S5B and S5C). We found such large indels in 5 of 8 screened genes, demonstrating that, for these genes, our screen was sensitive enough to detect animals with affected phenotypes (Table S2).

From the screen, we isolated 57 alleles for 3 genes (*egl-30*, *sqt-2*, and *sqt-3*) and none for the other 5 genes (*dpy-2*, *dpy-10*, *rol-6*, *unc-26*, and *unc-54*) (Table S2). All alleles showed phenotypic defects described previously for a reduction of function of the affected genes. Deletions, insertions, and complex mutations (combination of insertions and deletions) were represented equally among isolates (Figure S5D). The observed phenotypic traits showed complete penetrance, and we scored their expression, which differed between mutations. We found that several mutations in the 3′ UTR of *egl-30* resulted in the Sluggish (Slu) phenotype, which is characterized by slow movement. In 7 of 11 mutants, a region around 100 bp downstream of the stop codon was affected, and the smallest deletion was 6 bp (Figures 5B and S5F). We found mutations overlapping a putative *sqt-2* enhancer predicted from chromatin accessibility profiling (Jänes et al., 2018) with a Roller (Rol) phenotype, where animals rotate around their body axis and move in circles (Figure S5E). This was the only region for which penetrance varied between different mutations. We also targeted *sqt-3*, a gene associated with three distinct morphological traits (Dpy, Rol, and Lon) (Cox et al., 1980; Kusch and Edgar, 1986). 13 mutations upstream of *sqt-3* likely affected transcriptional initiation, with 11 of 13 overlapping the predicted TATA box (Figure 5C). In line with the Rol phenotype, which indicates a reduction of function, pre-mRNA and mRNA levels were reduced to around half (Figure S5I). This suggests that *sqt-3* transcription partially tolerates removal of this core promoter element.

The 26 other isolated *sqt-3* alleles were 3′ UTR mutations. Almost all (25 of 26) were insertions or insertions combined with deletions, originating at sg2 (Figure 5D). The only deletion overlapped with a canonical polyadenylation signal (AATAAA). We knew from sequencing siblings that sg2 was very efficient (~25%) and that various deletions covering the 3′ UTR were present in our samples. We therefore isolated 13 distinct non-Rol mutants using direct PCR screening (Figures S5G). Despite

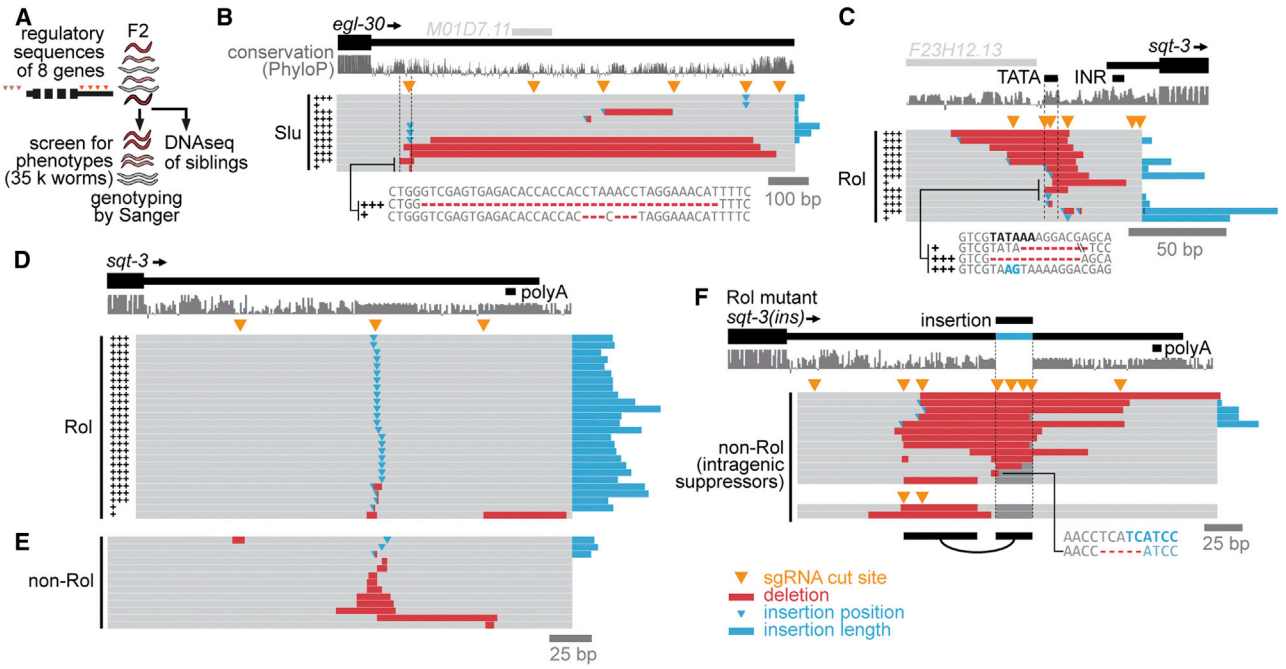


**Figure 5. Screening for functional regulatory sequences using morphological phenotypes**

Shown are genotypes of strains that were isolated according to phenotypic traits after targeting regulatory regions. Phenotypes showed complete penetrance (n > 300 animals), and expression was scored as indicated by +, ++, or +++ (n > 300 animals).

(A) Outline of the screen. 8 genes were targeted by pools of 2–6 sgRNAs in different regulatory regions (some enhancer, promoter, all 3′ UTRs), resulting in 21 samples. 35,000 F2 animals were screened manually for morphological traits.

(B) Eleven mutations along the *egl-30* 3′ UTR that show slight or strong Sluggish (Slu) phenotypes. No canonical polyadenylation signal could be found.

(C) Thirteen mutations upstream of *sqt-3* that show a Roller (Rol) phenotype.

(D) Mutations in the *sqt-3* 3′ UTR that show a Rol phenotype or are tolerated (non-Rol). "poly(A)" indicates the canonical polyadenylation signal AATAAA.

(E) Fifteen mutations, mostly deletions, that suppressed the Rol phenotype of one insertion allele *sqt-3(ins)*. Black bars at the bottom, uncovered compensatory interaction.

See also Figure S5.

containing indels originating at the efficient sg2, these animals showed the wild-type non-Rol trait (Figure 5E). We did follow-up experiments with one of the 25 insertion alleles, *sqt-3(ins)*, and determined that mRNA levels were reduced post-transcriptionally to around 50% (Figure S5H and S5I). Because deletions and some insertions in this region were well tolerated (non-Rol), we concluded that the isolated Rol mutations likely resulted from a gain of repressive sequence that led to the observed reduction of mRNA. The poly(A) mutant *sqt-3(polyA)*, for which mRNA levels were reduced equally to 50%, showed a weaker Rol phenotype than *sqt-3(ins)* with only slight bending of the head (Figures 5D, S5I, and S5J). This suggests that in addition to mRNA downregulation, other mechanisms might further reduce protein output in *sqt-3(ins).*

To define the repressive sequence elements in *sqt-3(ins)*, we targeted the inserted sequence with several sgRNAs and screened for revertants, in which the wild-type non-Rol trait was restored by intragenic suppressor mutations. 12 of 13 revertants contained deletions overlapping the insertion, with the smallest being 5 bp (Figure 5F). A restored wild-type trait likely resulted from restored expression levels. Indeed, mRNA levels in two independent revertants were restored to normal (Figure S5L). Overall, the predicted RNA secondary structures did not change, suggesting that other factors caused the Rol phenotype of *sqt-3(ins)* (Figure S5M). Finally, we wanted to test whether the repressive sequence could function in other genes. We performed sequence transplantations into the 3′ UTR of *dpy-10* and *unc-22*, of which only *unc-22* showed the characteristic reduction-of-function Twitcher phenotype (Figure S5N). These results indicated that the repressive sequence might also function in other contexts, but more experiments would be needed to test this thoroughly.

To discover other interacting regulatory sequences, we included sgRNAs for the remaining 3′ UTR and isolated non-Rol revertants that contained intragenic suppressor mutations. This revealed a compensatory deletion upstream of the insertion that was able to revert the Rol phenotype. We isolated two additional alleles after using sgRNAs specific for this region (Figures 5F and S5K). Surprisingly, mRNA levels were not restored (Figure S5L). This points to an alternative mechanism of restored protein function; for example, affecting translation or mRNA localization.

Overall, these results demonstrate that parallel genetics and selection by phenotype can be used to find functional sequences,

isolate a variety of mutant genotypes for follow-up studies, and discover unexpected intragenic regulatory interactions *in vivo*.

## DISCUSSION

In this study, we developed a general approach for parallel genetics of regulatory sequences *in vivo*, using inducible expression of a CRISPR nuclease and multiplexed sgRNAs. Large ''diversified'' populations can then be used for comprehensive analysis using deep sequencing and for selection by phenotypic traits or reporter expression. This allows directly linking regulatory genotypes with phenotypes. We demonstrate this in the model organism *C. elegans* but believe that it could be similarly applicable in other animals that allow transgenesis and inducible expression of genome editors.

As we show, sgRNA efficiencies around 1.5% are sufficient to analyze effects of mutations on gene regulation and phenotype when coupled with deep sequencing and manual or automated selection of animals from large populations. However, higher efficiency would be desired for improved comprehensive testing. This could already be achieved with available improved expression systems (Aljohani et al., 2020; Nance and Frøkjær-Jensen, 2019). Alternative induction systems could enable continuous and germline-specific Cas9 expression to further increase efficiency and allow directed evolution experiments (Nance and Frøkjær-Jensen, 2019; Zhang et al., 2015). Our method only works at nucleotide resolution close to the sgRNA cut sites. To allow denser tiling of regions with mutations, CRISPR nucleases with alternative or dispensable PAM requirements could be used (Anzalone et al., 2020; Chatterjee et al., 2020; Walton et al., 2020). Although indels are applicable to regulatory regions and even coding sequences (He et al., 2019; Sher et al., 2019; Shi et al., 2015), point mutagenesis would enable fine mapping of regulatory nucleotides and coding sequences. This exciting possibility could be realized by implementing hyperactive base editors (Chen et al., 2019a; Hess et al., 2016; Li et al., 2020; Ma et al., 2016) or programmable *in situ* production of single-stranded DNA templates from sgRNAs (Anzalone et al., 2019; Sharon et al., 2018). Alternatives to CRISPR-Cas could be developed based on inducible recombinase-mediated cassette exchange (Hubbard, 2014; Macías-León and Askjaer, 2018; Nonet, 2020) or transposon-mediated single-copy insertion (Frøkjær-Jensen et al., 2012, 2014) to integrate variant libraries in parallel. Targeting several independent loci in one step might be applied to screen candidate regulatory elements (for example, miRNA targets or enhancers), to screen genes from networks or pathways, or for synthetic co-evolution of several loci (Simon et al., 2019).

Our targeted sequencing protocol can capture long deletions, uses the same amplicon for the whole locus, and allows sample multiplexing. Unique molecule-counting methods for long reads should be incorporated to reduce PCR bias (Karst et al., 2021; McCoy et al., 2014). Established protocols are available for shorter (100- to 300-bp) target regions (Chen et al., 2019b). We assumed that each animal in bulk samples contributed equally to the extracted genomic DNA. In the future, animal barcoding to determine genotypes of individuals could be added, with plate-based or split-pool methods (Cao et al., 2017; Rosenberg et al., 2018).

Indel data from high-throughput genome editing in human cells has led to insights into dsDNA break repair outcomes (Allen et al., 2018; Chakrabarti et al., 2019; Chen et al., 2019b; Leenay et al., 2019; Shen et al., 2018; Shou et al., 2018). We found longer indels and fewer 1-nt templated insertions in our data. This can likely be explained by a higher activity of microhomology-mediated end joining (MMEJ), which uses 5- to 25-bp microhomologies and has been reported as the main dsDNA break repair pathway in *C. elegans* (van Schendel et al., 2015). Mutations typical for MMEJ have been implicated in diseases (Schimmel et al., 2019), and our approach to produce deep mutation profiles could be used to study mechanisms of MMEJ in the germline.

Gain or loss of regulatory sequences is important for determination and evolution of phenotypes (Davidson, 2010; Wittkopp and Kalay, 2011; Wray et al., 2003). Mutational effect can be modeled as a gradual process by single-nucleotide changes (Chen and Rajewsky, 2007; Hardison and Taylor, 2012; Romero et al., 2012; Wittkopp and Kalay, 2011; Wray, 2007; Wray et al., 2003). However, although indels occur less often, their effects can be more severe. We found that insertions contained sequences surrounding the dsDNA break, mainly in the same orientation. Such local duplications could have particular strong consequences when functional sequences are multiplied.

Using targeted RNA and DNA sequencing in bulk populations, we quantified the effect of *lin-41* 3′ UTR deletions on mRNA expression and fitness effect. High-throughput methods to determine single-animal genotypes could improve statistical power, and single-cell RNA sequencing could be used to detect cell-type- or tissue-specific effects. We found that each *let-7* site could function on its own. In contrast, previous studies had concluded that one binding site could not function alone to repress an extra-chromosomal LacZ protein reporter (Vella et al., 2004a) or tested only multiple copies of each site (Long et al., 2007; Vella et al., 2004b). We found a stronger effect on mRNA regulation and phenotype when disrupting *let-7* binding site 1 compared with site 2. Supporting this, site 1 has a longer seed pairing (8 nt) than site 2 (6 nt and a G-U pair) and was covered with more reads in an *in vivo* miRNA proximity ligation approach (Broughton et al., 2016). Surprisingly, site 2 mutants did not show any obvious morphological defects or a bursting/lethal phenotype. Future studies could investigate the detailed function of each site and possible compensatory mechanisms.

Our screen for sequences that affect phenotypic traits doubles the regulatory alleles registered at Wormbase in the last 40 years (Harris et al., 2020). Our approach can be applied to isolate animals with altered expression and phenotypic traits, which is useful to identify functional sequences and study the regulation of animal phenotype. Our results also highlight the possibility of uncovering unexpected intragenic regulatory interactions using readout of phenotype. Because of the mutagenesis efficiency and because we screened for strong phenotypes, we did not saturate and likely missed many mutations. To determine comprehensively which mutations are tolerated by a locus, even higher efficiencies would be needed.

We believe that the approaches presented here will help with understanding how gene-regulatory logic and mechanisms affect phenotypes *in vivo*.

## STAR★METHODS

Detailed methods are provided in the online version of this paper and include the following:

- KEY RESOURCES TABLE
- RESOURCE AVAILABILITY
  - Lead contact
  - Materials availability
  - Data and code availability
- EXPERIMENTAL MODEL AND SUBJECT DETAILS
  - *Caenorhabditis elegans*
- METHOD DETAILS
  - Plasmid construction
  - sgRNA design
  - Generation of transgenic *C. elegans*
  - C-terminal GFP knock-in of *his-72*
  - Biosorter
  - Small-scale Cas9 induction and time course
  - Developmental synchronization
  - Large-scale Cas9 heat shock induction
  - Genomic DNA extraction
  - DNA long amplicon sequencing
  - The crispr-DART software
  - Steps of the crispr-DART software
  - Browser shots
  - sgRNA efficiency comparisons
  - Indel characteristics
  - Genotype diversity
  - Targeted mRNA sequencing, *lin-41*
  - RNA analysis of *lin-41* 3′ UTR deletions
  - RNA analysis by unsupervised clustering of long reads
  - DNA sampling over generations, *lin-41*
  - Fitness analysis of *lin-41* 3′ UTR deletions
  - *Lin-41* strains with site1 or site2 deletions
  - Screen for regulatory sequences by phenotype
  - PCR Genotyping
  - *Sqt-3* mRNA quantifications by Nanostring or qPCR
  - Transplantations into *dpy-10*, *unc-22* 3′ UTRs
- QUANTIFICATION AND STATISTICAL ANALYSIS

## SUPPLEMENTAL INFORMATION

Supplemental information can be found online at https://doi.org/10.1016/j.celrep.2021.108988.

## ACKNOWLEDGMENTS

We are very grateful to Baris Tursun and Luisa Cochella for in-depth comments and discussion. We thank David Koppstein and the Rajewsky and Akalin labs for helpful feedback and discussions and Claudia Quedenau, Daniele Franze, the sequencing facility for Pacbio sequencing, Sergej Herzog, and Salah Ayoub for technical assistance. For sharing plasmids and strains, we thank João Ramalho, Mike Boxem, Jason Chin, Christian Frøkjaer-Jensen, Erik Jorgensen, Daniel Dickinson, Bob Goldstein, and the Caenorhabditis Genetics Center (CGC), funded by the NIH Office of Research Infrastructure Programs P40 OD010440. B.U. acknowledges funding from the German Federal Ministry of Education and Research (BMBF) as part of the RNA Bioinformatics Center of the German Network for Bioinformatics Infrastructure (de.NBI; 031 A538C RBC). J.J.F. was supported by funding from the German Research Foundation (DFG; RA 838/5-1 and RA 838/11-1). Part of this work was supported by the Leibniz Prize of the German Research Foundation awarded to N.R. (DFG; RA 838/5-1)

## AUTHOR CONTRIBUTIONS

J.J.F. and N.R. developed concepts and methodology and discussed the data. J.J.F. and B.U. performed validation, formal analysis, curation, and visualization of data. B.U. wrote the software with input from J.J.F. and A.A., and P.G. contributed to the software. J.J.F., M.H., and K.T. performed investigations and experimental work. J.J.F. and N.R. assembled figures, wrote the original draft, and revised the manuscript. J.J.F., B.U., A.A., and N.R. reviewed and edited the manuscript. A.A. and N.R. contributed resources, supervision, project administration, and funding acquisition.

## DECLARATION OF INTERESTS

The authors declare no competing interests.

Received: August 24, 2020
Revised: January 13, 2021
Accepted: March 23, 2021
Published: April 13, 2021

## REFERENCES

Abbott, A.L., Alvarez-Saavedra, E., Miska, E.A., Lau, N.C., Bartel, D.P., Horvitz, H.R., and Ambros, V. (2005). The let-7 MicroRNA family members mir-48, mir-84, and mir-241 function together to regulate developmental timing in Caenorhabditis elegans. Dev. Cell *9*, 403–414.

Adikusuma, F., Piltz, S., Corbett, M.A., Turvey, M., McColl, S.R., Helbig, K.J., Beard, M.R., Hughes, J., Pomerantz, R.T., and Thomas, P.Q. (2018). Large deletions induced by Cas9 cleavage. Nature *560*, E8–E9.

Aeschimann, F., Kumari, P., Bartake, H., Gaidatzis, D., Xu, L., Ciosk, R., and Großhans, H. (2017). LIN41 Post-transcriptionally Silences mRNAs by Two Distinct and Position-Dependent Mechanisms. Mol. Cell *65*, 476–489.e4.

Aljohani, M.D., El Mouridi, S., Priyadarshini, M., Vargas-Velazquez, A.M., and Frøkjær-Jensen, C. (2020). Engineering rules that minimize germline silencing of transgenes in simple extrachromosomal arrays in C. elegans. Nat. Commun. *11*, 6300.

Allen, F., Crepaldi, L., Alsinet, C., Strong, A.J., Kleshchevnikov, V., De Angeli, P., Páleníková, P., Khodak, A., Kiselev, V., Kosicki, M., et al. (2018). Predicting the mutations generated by repair of Cas9-induced double-strand breaks. Nat. Biotechnol. *37*, 64–72.

Anzalone, A.V., Randolph, P.B., Davis, J.R., Sousa, A.A., Koblan, L.W., Levy, J.M., Chen, P.J., Wilson, C., Newby, G.A., Raguram, A., and Liu, D.R. (2019). Search-and-replace genome editing without double-strand breaks or donor DNA. Nature *576*, 149–157.

Anzalone, A.V., Koblan, L.W., and Liu, D.R. (2020). Genome editing with CRISPR-Cas nucleases, base editors, transposases and prime. Nat. Biotechnol. *38*, 824–844.

Bagga, S., Bracht, J., Hunter, S., Massirer, K., Holtz, J., Eachus, R., and Pasquinelli, A.E. (2005). Regulation by let-7 and lin-4 miRNAs results in target mRNA degradation. Cell *122*, 553–563.

Barrangou, R., and Doudna, J.A. (2016). Applications of CRISPR technologies in research and beyond. Nat. Biotechnol. *34*, 933–941.

Brancati, G., and Großhans, H. (2018). An interplay of miRNA abundance and target site architecture determines miRNA activity and specificity. Nucleic Acids Res. *46*, 3259–3269.

Brenner, S. (1974). The genetics of Caenorhabditis elegans. Genetics *77*, 71–94.

Broughton, J.P., Lovci, M.T., Huang, J.L., Yeo, G.W., and Pasquinelli, A.E. (2016). Pairing beyond the Seed Supports MicroRNA Targeting Specificity. Mol. Cell *64*, 320–333.

Burga, A., and Lehner, B. (2012). Beyond genotype to phenotype: why the phenotype of an individual cannot always be predicted from their genome sequence and the environment that they experience. FEBS J. *279*, 3765–3775.

Bushnell, B. (2014). BBMap: A Fast, Accurate, Splice-Aware Aligner (Lawrence Berkeley National Laboratory. LBNL Report LBNL-7065E). https://jgi.doe.gov/wp-content/uploads/2013/11/BB_User-Meeting-2014-poster-FINAL.pdf.

Canver, M.C., Smith, E.C., Sher, F., Pinello, L., Sanjana, N.E., Shalem, O., Chen, D.D., Schupp, P.G., Vinjamur, D.S., Garcia, S.P., et al. (2015). BCL11A enhancer dissection by Cas9-mediated in situ saturating mutagenesis. Nature *527*, 192–197.

Cao, J., Packer, J.S., Ramani, V., Cusanovich, D.A., Huynh, C., Daza, R., Qiu, X., Lee, C., Furlan, S.N., Steemers, F.J., et al. (2017). Comprehensive single-cell transcriptional profiling of a multicellular organism. Science *357*, 661–667.

Chakrabarti, A.M., Henser-Brownhill, T., Monserrat, J., Poetsch, A.R., Luscombe, N.M., and Scaffidi, P. (2019). Target-Specific Precision of CRISPR-Mediated Genome Editing. Mol. Cell *73*, 699–713.e6.

Chatterjee, P., Jakimo, N., Lee, J., Amrani, N., Rodríguez, T., Koseki, S.R.T., Tysinger, E., Qing, R., Hao, S., Sontheimer, E.J., et al. (2020). An engineered ScCas9 with broad PAM range and high specificity and activity. Nat. Biotechnol. *38*, 1154–1158.

Chen, K., and Rajewsky, N. (2007). The evolution of gene regulation by transcription factors and microRNAs. Nat. Rev. Genet. *8*, 93–103.

Chen, H., Liu, S., Padula, S., Lesman, D., Griswold, K., Lin, A., Zhao, T., Marshall, J.L., and Chen, F. (2019a). Efficient, continuous mutagenesis in human cells using a pseudo-random DNA. Nat. Biotechnol. *38*, 165–168.

Chen, W., McKenna, A., Schreiber, J., Haeussler, M., Yin, Y., Agarwal, V., Noble, W.S., and Shendure, J. (2019b). Massively parallel profiling and predictive modeling of the outcomes of CRISPR/Cas9-mediated double-strand break repair. Nucleic Acids Res. *47*, 7989–8003.

Collins, R.L., Brand, H., Karczewski, K.J., Zhao, X., Alföldi, J., Francioli, L.C., Khera, A.V., Lowther, C., Gauthier, L.D., Wang, H., et al.; Genome Aggregation Database Production Team; Genome Aggregation Database Consortium (2020). A structural variation reference for medical and population genetics. Nature *581*, 444–451.

Cox, G.N., Laufer, J.S., Kusch, M., and Edgar, R.S. (1980). Genetic and Phenotypic Characterization of Roller Mutants of CAENORHABDITIS ELEGANS. Genetics *95*, 317–339.

Davidson, E.H. (2010). The Regulatory Genome: Gene Regulatory Networks in Development And Evolution (Elsevier).

DePristo, M.A., Banks, E., Poplin, R., Garimella, K.V., Maguire, J.R., Hartl, C., Philippakis, A.A., del Angel, G., Rivas, M.A., Hanna, M., et al. (2011). A framework for variation discovery and genotyping using next-generation DNA sequencing data. Nat. Genet. *43*, 491–498.

Diag, A., Schilling, M., Klironomos, F., Ayoub, S., and Rajewsky, N. (2018). Spatiotemporal m(i)RNA Architecture and 3′ UTR Regulation in the C. elegans Germline. Dev. Cell *47*, 785–800.e8.

Dickinson, D.J., Pani, A.M., Heppert, J.K., Higgins, C.D., and Goldstein, B. (2015). Streamlined Genome Engineering with a Self-Excising Drug Selection Cassette. Genetics *200*, 1035–1049.

Dominguez, D., Freese, P., Alexis, M.S., Su, A., Hochman, M., Palden, T., Bazile, C., Lambert, N.J., Van Nostrand, E.L., Pratt, G.A., et al. (2018). Sequence, Structure, and Context Preferences of Human RNA Binding Proteins. Mol. Cell *70*, 854–867.e9.

Ecsedi, M., Rausch, M., and Großhans, H. (2015). The let-7 microRNA directs vulval development through a single target. Dev. Cell *32*, 335–344.

Ewels, P., Magnusson, M., Lundin, S., and Käller, M. (2016). MultiQC: summarize analysis results for multiple tools and samples in a single report. Bioinformatics *32*, 3047–3048.

Farboud, B., and Meyer, B.J. (2015). Dramatic Enhancement of Genome Editing by CRISPR/Cas9 Through Improved Guide RNA Design. Genetics *199*, 959–971.

Farley, E.K., Olson, K.M., Zhang, W., Brandt, A.J., Rokhsar, D.S., and Levine, M.S. (2015). Suboptimization of developmental enhancers. Science *350*, 325–328.

Fatt, H.V., and Dougherty, E.C. (1963). Genetic Control of Differential Heat Tolerance in Two Strains of the Nematode Caenorhabditis elegans. Science *141*, 266–267.

Findlay, G.M., Boyle, E.A., Hause, R.J., Klein, J.C., and Shendure, J. (2014). Saturation editing of genomic regions by multiplex homology-directed repair. Nature *513*, 120–123.

Friedland, A.E., Tzur, Y.B., Esvelt, K.M., Colaiácovo, M.P., Church, G.M., and Calarco, J.A. (2013). Heritable genome editing in C. elegans via a CRISPR-Cas9 system. Nat. Methods *10*, 741–743.

Frøkjaer-Jensen, C., Davis, M.W., Hopkins, C.E., Newman, B.J., Thummel, J.M., Olesen, S.-P., Grunnet, M., and Jorgensen, E.M. (2008). Single-copy insertion of transgenes in Caenorhabditis elegans. Nat. Genet. *40*, 1375–1383.

Frøkjær-Jensen, C., Davis, M.W., Ailion, M., and Jorgensen, E.M. (2012). Improved Mos1-mediated transgenesis in C. elegans. Nat. Methods *9*, 117–118.

Frøkjær-Jensen, C., Davis, M.W., Sarov, M., Taylor, J., Flibotte, S., LaBella, M., Pozniakovsky, A., Moerman, D.G., and Jorgensen, E.M. (2014). Random and targeted transgene insertion in Caenorhabditis elegans using a modified Mos1 transposon. Nat. Methods *11*, 529–534.

Fuqua, T., Jordan, J., van Breugel, M.E., Halavatyi, A., Tischer, C., Polidoro, P., Abe, N., Tsai, A., Mann, R.S., Stern, D.L., and Crocker, J. (2020). Dense and pleiotropic regulatory information in a developmental enhancer. Nature *587*, 235–239.

Gasperini, M., Starita, L., and Shendure, J. (2016). The power of multiplexed functional analysis of genetic variants. Nat. Protoc. *11*, 1782–1787.

Gasperini, M., Findlay, G.M., McKenna, A., Milbank, J.H., Lee, C., Zhang, M.D., Cusanovich, D.A., and Shendure, J. (2017). CRISPR/Cas9-Mediated Scanning for Regulatory Elements Required for HPRT1 Expression via Thousands of Large, Programmed Genomic Deletions. Am. J. Hum. Genet. *101*, 192–205.

Gibson, D.G., Young, L., Chuang, R.-Y., Venter, J.C., Hutchison, C.A., 3rd, and Smith, H.O. (2009). Enzymatic assembly of DNA molecules up to several hundred kilobases. Nat. Methods *6*, 343–345.

Haeussler, M., Schönig, K., Eckert, H., Eschstruth, A., Mianné, J., Renaud, J.-B., Schneider-Maunoury, S., Shkumatava, A., Teboul, L., Kent, J., et al. (2016). Evaluation of off-target and on-target scoring algorithms and integration into the guide RNA selection tool CRISPOR. Genome Biol. *17*, 148.

Hardison, R.C., and Taylor, J. (2012). Genomic approaches towards finding cis-regulatory modules in animals. Nat. Rev. Genet. *13*, 469–483.

Harris, T.W., Arnaboldi, V., Cain, S., Chan, J., Chen, W.J., Cho, J., Davis, P., Gao, S., Grove, C.A., Kishore, R., et al. (2020). WormBase: a modern Model Organism Information Resource. Nucleic Acids Res. *48* (*D1*), D762–D767.

He, W., Zhang, L., Villarreal, O.D., Fu, R., Bedford, E., Dou, J., Patel, A.Y., Bedford, M.T., Shi, X., Chen, T., et al. (2019). De novo identification of essential protein domains from CRISPR-Cas9 tiling-sgRNA knockout screens. Nat. Commun. *10*, 4541.

Heigwer, F., Kerr, G., and Boutros, M. (2014). E-CRISP: fast CRISPR target site identification. Nat. Methods *11*, 122–123.

Hess, G.T., Frésard, L., Han, K., Lee, C.H., Li, A., Cimprich, K.A., Montgomery, S.B., and Bassik, M.C. (2016). Directed evolution using dCas9-targeted somatic hypermutation in mammalian cells. Nat. Methods *13*, 1036–1042.

Hörnblad, A., Bastide, S., Langenfeld, K., Langa, F., and Spitz, F. (2021). Dissection of the Fgf8 regulatory landscape by in vivo CRISPR-editing reveals extensive inter- and intra-enhancer redundancy. Nat. Commun. *12*, 439.

Hubbard, E.J.A. (2014). FLP/FRT and Cre/lox recombination technology in C. elegans. Methods *68*, 417–424.

Hunter, S.E., Finnegan, E.F., Zisoulis, D.G., Lovci, M.T., Melnik-Martinez, K.V., Yeo, G.W., and Pasquinelli, A.E. (2013). Functional genomic analysis of the let-7 regulatory network in Caenorhabditis elegans. PLoS Genet. *9*, e1003353.

Jänes, J., Dong, Y., Schoof, M., Serizay, J., Appert, A., Cerrato, C., Woodbury, C., Chen, R., Gemma, C., Huang, N., et al. (2018). Chromatin accessibility dynamics across *C. elegans* development and ageing. eLife *7*, e37344.

Jankowsky, E., and Harris, M.E. (2015). Specificity and nonspecificity in RNA-protein interactions. Nat. Rev. Mol. Cell Biol. *16*, 533–544.

Karst, S.M., Ziels, R.M., Kirkegaard, R.H., Sørensen, E.A., McDonald, D., Zhu, Q., Knight, R., and Albertsen, M. (2021). High-accuracy long-read amplicon sequences using unique molecular identifiers with Nanopore or PacBio sequencing. Nat. Methods *18*, 165–169.

Kent, W.J., Sugnet, C.W., Furey, T.S., Roskin, K.M., Pringle, T.H., Zahler, A.M., and Haussler, D. (2002). The human genome browser at UCSC. Genome Res. *12*, 996–1006.

Konrad, A., Brady, M.J., Bergthorsson, U., and Katju, V. (2019). Mutational Landscape of Spontaneous Base Substitutions and Small Indels in Experimental *Caenorhabditis elegans* Populations of Differing Size. Genetics *212*, 837–854.

Kontarakis, Z., and Stainier, D.Y.R. (2020). Genetics in Light of Transcriptional Adaptation. Trends Genet. *36*, 926–935.

Kosicki, M., Tomberg, K., and Bradley, A. (2018). Repair of double-strand breaks induced by CRISPR-Cas9 leads to large deletions and complex rearrangements. Nat. Biotechnol. *36*, 765–771.

Köster, J., and Rahmann, S. (2012). Snakemake–a scalable bioinformatics workflow engine. Bioinformatics *28*, 2520–2522.

Kusch, M., and Edgar, R.S. (1986). Genetic studies of unusual loci that affect body shape of the nematode Caenorhabditis elegans and may code for cuticle structural proteins. Genetics *113*, 621–639.

Kvon, E.Z., Zhu, Y., Kelman, G., Novak, C.S., Plajzer-Frick, I., Kato, M., Garvin, T.H., Pham, Q., Harrington, A.N., Hunter, R.D., et al. (2020). Comprehensive In Vivo Interrogation Reveals Phenotypic Impact of Human Enhancer Variants. Cell *180*, 1262–1271.e15.

Labi, V., Peng, S., Klironomos, F., Munschauer, M., Kastelic, N., Chakraborty, T., Schoeler, K., Derudder, E., Martella, M., Mastrobuoni, G., et al. (2019). Context-specific regulation of cell survival by a miRNA-controlled BIM rheostat. Genes Dev. *33*, 1673–1687.

Lawrence, M., Huber, W., Pagès, H., Aboyoun, P., Carlson, M., Gentleman, R., Morgan, M.T., and Carey, V.J. (2013). Software for computing and annotating genomic ranges. PLoS Comput. Biol. *9*, e1003118.

Leenay, R.T., Aghazadeh, A., Hiatt, J., Tse, D., Roth, T.L., Apathy, R., Shifrut, E., Hultquist, J.F., Krogan, N., Wu, Z., et al. (2019). Large dataset enables prediction of repair after CRISPR-Cas9 editing in primary T cells. Nat. Biotechnol. *37*, 1034–1037.

Levo, M., and Segal, E. (2014). In pursuit of design principles of regulatory sequences. Nat. Rev. Genet. *15*, 453–468.

Li, C., Zhang, R., Meng, X., Chen, S., Zong, Y., Lu, C., Qiu, J.-L., Chen, Y.-H., Li, J., and Gao, C. (2020). Targeted, random mutagenesis of plant genes with dual cytosine and adenine base. Nat. Biotechnol. *38*, 875–882.

Long, D., Lee, R., Williams, P., Chan, C.Y., Ambros, V., and Ding, Y. (2007). Potent effect of target structure on microRNA function. Nat. Struct. Mol. Biol. *14*, 287–294.

Long, H.K., Prescott, S.L., and Wysocka, J. (2016). Ever-Changing Landscapes: Transcriptional Enhancers in Development and Evolution. Cell *167*, 1170–1187.

Ma, Y., Zhang, J., Yin, W., Zhang, Z., Song, Y., and Chang, X. (2016). Targeted AID-mediated mutagenesis (TAM) enables efficient genomic diversification in mammalian cells. Nat. Methods *13*, 1029–1035.

Macías-León, J., and Askjaer, P. (2018). Efficient FLP-mediated germ-line recombination in C. elegans (MicroPublication Biology).

Macneil, L.T., and Walhout, A.J.M. (2011). Gene regulatory networks and the role of robustness and stochasticity in the control of gene expression. Genome Res. *21*, 645–657.

McCoy, R.C., Taylor, R.W., Blauwkamp, T.A., Kelley, J.L., Kertesz, M., Pushkarev, D., Petrov, D.A., and Fiston-Lavier, A.-S. (2014). Illumina TruSeq synthetic long-reads empower de novo assembly and resolve complex, highly-repetitive transposable elements. PLoS ONE *9*, e106689.

Mello, C., and Fire, A. (1995). DNA transformation. Methods Cell Biol. *48*, 451–482.

Morgan, M., Pagès, H., Obenchain, V., and Hayden, N. (2020). Rsamtools: Binary alignment (BAM), FASTA, variant call (BCF), and tabix file import (Bioconductor version Release 3.12). R package version 2.6.0. https://bioconductor.org/packages/Rsamtools.

Nance, J., and Frøkjær-Jensen, C. (2019). The *Caenorhabditis elegans* Transgenic Toolbox. Genetics *212*, 959–990.

Nonet, M.L. (2020). Efficient Transgenesis in *Caenorhabditis elegans* Using Flp Recombinase-Mediated Cassette Exchange. Genetics *215*, 903–921.

Pagès, H., Aboyoun, P., Gentleman, R., and DebRoy, S. (2020). Biostrings: Efficient manipulation of biological strings. R package version 2.58.0. https://bioconductor.org/packages/Biostrings.

Rabani, M., Pieper, L., Chew, G.-L., and Schier, A.F. (2017). A Massively Parallel Reporter Assay of 3′ UTR Sequences Identifies In Vivo Rules for mRNA Degradation. Mol. Cell *68*, 1083–1094.e5.

Radman, I., Greiss, S., and Chin, J.W. (2013). Efficient and rapid C. elegans transgenesis by bombardment and hygromycin B selection. PLoS ONE *8*, e76019.

Reinhart, B.J., Slack, F.J., Basson, M., Pasquinelli, A.E., Bettinger, J.C., Rougvie, A.E., Horvitz, H.R., and Ruvkun, G. (2000). The 21-nucleotide let-7 RNA regulates developmental timing in Caenorhabditis elegans. Nature *403*, 901–906.

Robinson, J.T., Thorvaldsdóttir, H., Winckler, W., Guttman, M., Lander, E.S., Getz, G., and Mesirov, J.P. (2011). Integrative genomics viewer. Nat. Biotechnol. *29*, 24–26.

Romero, I.G., Ruvinsky, I., and Gilad, Y. (2012). Comparative studies of gene expression and the evolution of gene regulation. Nat. Rev. Genet. *13*, 505–516.

Rosenberg, A.B., Roco, C.M., Muscat, R.A., Kuchina, A., Sample, P., Yao, Z., Graybuck, L.T., Peeler, D.J., Mukherjee, S., Chen, W., et al. (2018). Single-cell profiling of the developing mouse brain and spinal cord with split-pool barcoding. Science *360*, 176–182.

Schimmel, J., van Schendel, R., den Dunnen, J.T., and Tijsterman, M. (2019). Templated Insertions: A Smoking Gun for Polymerase Theta-Mediated End Joining. Trends Genet. *35*, 632–644.

Sharon, E., Chen, S.-A.A., Khosla, N.M., Smith, J.D., Pritchard, J.K., and Fraser, H.B. (2018). Functional Genetic Variants Revealed by Massively Parallel Precise Genome Editing. Cell *175*, 544–557.e16.

Shen, M.W., Arbab, M., Hsu, J.Y., Worstell, D., Culbertson, S.J., Krabbe, O., Cassa, C.A., Liu, D.R., Gifford, D.K., and Sherwood, R.I. (2018). Predictable and precise template-free CRISPR editing of pathogenic variants. Nature *563*, 646–651.

Shendure, J., and Fields, S. (2016). Massively Parallel Genetics. Genetics *203*, 617–619.

Sher, F., Hossain, M., Seruggia, D., Schoonenberg, V.A.C., Yao, Q., Cifani, P., Dassama, L.M.K., Cole, M.A., Ren, C., Vinjamur, D.S., et al. (2019). Rational targeting of a NuRD subcomplex guided by comprehensive in situ mutagenesis. Nat. Genet. *51*, 1149–1159.

Shi, J., Wang, E., Milazzo, J.P., Wang, Z., Kinney, J.B., and Vakoc, C.R. (2015). Discovery of cancer drug targets by CRISPR-Cas9 screening of protein domains. Nat. Biotechnol. *33*, 661–667.

Shou, J., Li, J., Liu, Y., and Wu, Q. (2018). Precise and Predictable CRISPR Chromosomal Rearrangements Reveal Principles of Cas9-Mediated Nucleotide Insertion. Mol. Cell *71*, 498–509.e4.

Simon, A.J., d'Oelsnitz, S., and Ellington, A.D. (2019). Synthetic evolution. Nat. Biotechnol. *37*, 730–743.

Slack, F.J., Basson, M., Liu, Z., Ambros, V., Horvitz, H.R., and Ruvkun, G. (2000). The lin-41 RBCC gene acts in the C. elegans heterochronic pathway between the let-7 regulatory RNA and the LIN-29 transcription factor. Mol. Cell *5*, 659–669.

Smits, A.H., Ziebell, F., Joberty, G., Zinn, N., Mueller, W.F., Clauder-Münster, S., Eberhard, D., Fälth Savitski, M., Grandi, P., Jakob, P., et al. (2019). Biological plasticity rescues target activity in CRISPR knock outs. Nat. Methods *16*, 1087–1093.

Stuart, T., Butler, A., Hoffman, P., Hafemeister, C., Papalexi, E., Mauck, W.M., 3rd, Hao, Y., Stoeckius, M., Smibert, P., and Satija, R. (2019). Comprehensive Integration of Single-Cell Data. Cell *177*, 1888–1902.e21.

Sulston, J.E., and Hodgkin, J. (1988). The Nematode *Caenorhabditis elegans* (Cold Spring Harbor Laboratory Press), pp. 587–606.

van Schendel, R., Roerink, S.F., Portegijs, V., van den Heuvel, S., and Tijsterman, M. (2015). Polymerase Θ is a key driver of genome evolution and of CRISPR/Cas9-mediated mutagenesis. Nat. Commun. *6*, 7394.

Vella, M.C., Choi, E.-Y., Lin, S.-Y., Reinert, K., and Slack, F.J. (2004a). The C. elegans microRNA let-7 binds to imperfect let-7 complementary sites from the lin-41 3'UTR. Genes Dev. *18*, 132–137.

Vella, M.C., Reinert, K., and Slack, F.J. (2004b). Architecture of a validated microRNA:target interaction. Chem. Biol. *11*, 1619–1623.

Vierstra, J., Reik, A., Chang, K.-H., Stehling-Sun, S., Zhou, Y., Hinkley, S.J., Paschon, D.E., Zhang, L., Psatha, N., Bendana, Y.R., et al. (2015). Functional footprinting of regulatory DNA. Nat. Methods *12*, 927–930, advance online publication.

Waaijers, S., Portegijs, V., Kerver, J., Lemmens, B.B.L.G., Tijsterman, M., van den Heuvel, S., and Boxem, M. (2013). CRISPR/Cas9-targeted mutagenesis in Caenorhabditis elegans. Genetics *195*, 1187–1191.

Waaijers, S., Muñoz, J., Berends, C., Ramalho, J.J., Goerdayal, S.S., Low, T.Y., Zoumaro-Djayoon, A.D., Hoffmann, M., Koorman, T., Tas, R.P., et al. (2016). A tissue-specific protein purification approach in Caenorhabditis elegans identifies novel interaction partners of DLG-1/Discs large. BMC Biol. *14*, 66.

Walton, R.T., Christie, K.A., Whittaker, M.N., and Kleinstiver, B.P. (2020). Unconstrained genome targeting with near-PAMless engineered CRISPR-Cas9 variants. Science *368*, 290–296.

Wittkopp, P.J., and Kalay, G. (2011). Cis-regulatory elements: molecular mechanisms and evolutionary processes underlying divergence. Nat. Rev. Genet. *13*, 59–69.

Wray, G.A. (2007). The evolutionary significance of cis-regulatory mutations. Nat. Rev. Genet. *8*, 206–216.

Wray, G.A., Hahn, M.W., Abouheif, E., Balhoff, J.P., Pizer, M., Rockman, M.V., and Romano, L.A. (2003). The evolution of transcriptional regulation in eukaryotes. Mol. Biol. Evol. *20*, 1377–1419.

Wurmus, R., Uyar, B., Osberg, B., Franke, V., Gosdschan, A., Wreczycka, K., Ronen, J., and Akalin, A. (2018). PiGx: reproducible genomics analysis pipelines with GNU Guix. Gigascience *7*, giy123.

Xie, Y., Allaire, J.J., and Grolemund, G. (2018). R Markdown: The Definitive Guide (Chapman and Hall/CRC).

Yartseva, V., Takacs, C.M., Vejnar, C.E., Lee, M.T., and Giraldez, A.J. (2017). RESA identifies mRNA-regulatory sequences at high resolution. Nat. Methods *14*, 201–207.

Zhang, H., Artiles, K.L., and Fire, A.Z. (2015). Functional relevance of "seed" and "non-seed" sequences in microRNA-mediated promotion of C. elegans developmental progression. RNA *21*, 1980–1992.

Zhang, Liangyu, Ward, Jordan, D., Cheng, Ze, and Dernburg, Abby, F.. (2015). The auxin-inducible degradation (AID) system enables versatile conditional protein depletion in C. elegans. Development. https://doi.org/10.1242/dev.129635.

## STAR★METHODS

### KEY RESOURCES TABLE

| REAGENT or RESOURCE | SOURCE | IDENTIFIER |
|---|---|---|
| **Bacterial and virus strains** | | |
| *E. coli* OP50 | Caenorhabditis Genetics Center (CGC) | https://cgc.umn.edu/strain/OP50 |
| *E. coli* DH5alpha Mix & Go Competent Cells | Zymo | Cat#T3007 |
| *E. coli* One Shot ccdB Survival | Thermo Fisher | Cat#A10460 |
| **Chemicals, peptides, and recombinant proteins** | | |
| Hygromycin B | Thermo Fisher | Cat#10687010 |
| HiFi DNA Assembly Master Mix | NEB | Cat#E2621L |
| Fastdigest Eco31I | Thermo Fisher | Cat#FD0293 |
| Fastdigest BpiI | Thermo Fisher | Cat#FD1014 |
| T4 DNA ligase and buffer | Thermo Fisher | Cat#EL0011 |
| T4 PNK | Thermo Fisher | Cat#EK0031 |
| ZymoPURE Plasmid Miniprep kit | Zymo | Cat#D4208T |
| phenol/chlorophorm/isoamylacohol pH 8.0 | Carl Roth | Cat#A156 |
| RNase I | Thermo Fisher | Cat#EN0601 |
| Phusion HF polymerase | NEB | Cat#M0530L |
| TRIzol reagent | Thermo Fisher | Cat#15596-018 |
| Maxima H Minus Reverse Transcriptase | Thermo Fisher | Cat#EP0752 |
| Alt-R Cas9 V3 | IDT | Cat#1081058 |
| tracrRNA | IDT | Cat#1072532 |
| Blue S'Green qPCR Kit | Biozym | Cat#331416XL |
| **Critical commercial assays** | | |
| Qubit dsDNA HS kit | Thermo Fisher | Cat#Q32854 |
| Zymoclean Gel DNA Recovery Kit | Zymo | Cat#D4002 |
| AMPure XP Reagent | Beckman Coulter | Cat#A63881 |
| Nextera XT DNA kit | Illumina | Cat#FC-131-1096 |
| Miniseq Mid Output kit, 2x150 cycles | Illumina | Cat#FC-420-1004 |
| Nextseq 500 V2 Mid Output kit, 150 cycles | Illumina | Cat#FC-404-1001 |
| **Deposited data** | | |
| All raw sequencing data | This study | NCBI Bioproject: PRJNA701945 |
| All raw sequencing data - alternative repository | This study | https://bimsbstatic.mdc-berlin.de/akalin/buyar/froehlich_uyar_et_al_2020/reads.tgz |
| Sample sheet for running crispr-DART | This study | https://bimsbstatic.mdc-berlin.de/akalin/buyar/froehlich_uyar_et_al_2020/sample_sheet.csv |
| Output of crispr-DART | This study | https://bimsbstatic.mdc-berlin.de/akalin/buyar/froehlich_uyar_et_al_2020/crispr_dart_pipeline_output.tgz |
| HTML report of crispr-DART | This study | https://bimsbstatic.mdc-berlin.de/akalin/buyar/froehlich_uyar_et_al_2020/reports/index.html |
| *C. elegans* genome ce11 | Kent et al., 2002 | http://genome.ucsc.eduvia http://bioconductor.org/packages/release/data/annotation/html/BSgenome.Celegans.UCSC.ce11.html |

(*Continued on next page*)

*Continued*

| REAGENT or RESOURCE | SOURCE | IDENTIFIER |
|---|---|---|
| Experimental models: organisms/strains | | |
| See Table S3 for all *C. elegans* strains | Table S3 | N/A |
| Oligonucleotides | | |
| See Table S3 for all DNA oligonucleotides | Table S3 | N/A |
| Recombinant DNA | | |
| See Table S3 for all plasmids | Table S3 | N/A |
| pJJF152_Phsp_Cas9 | This study | Addgene #163862 |
| pJJF439_PU6_empty_sgRNAscaffold | This study | Addgene #164266 |
| pJJF143_SECGFP_sg1 | This study | Addgene #163864 |
| pJJF144_SECGFP_sg2 | This study | Addgene #163865 |
| pJJF449_dpy-10_CDS_sg1 | This study | Addgene #163866 |
| pJJF328_sqt-3_3′UTR_sg2 | This study | Addgene #163867 |
| pJJF496_dpy-10_CDS_sg6 (in pJJR50) | This study | Addgene #164267 |
| pJJF495_dpy-10_CDS_sg6 (in pJJF439) | This study | Addgene #164268 |
| Software and algorithms | | |
| crispr-DART | This study | https://github.com/BIMSBbioinfo/crispr_DART |
| code to reproduce analyses and figures | This study | https://github.com/BIMSBbioinfo/froehlich_uyar_et_al_2020 |
| CRISPOR | Haeussler et al., 2016 | https://crispor.tefor.net/ |
| E-CRISP | Heigwer et al., 2014 | http://www.e-crisp.org/E-CRISP |
| Ape (A plasmid Editor) | M.W. Davis | https://jorgensen.biology.utah.edu/wayned/ape/ |
| Snapgene | GSL Biotech | https://www.snapgene.com/ |
| Snakemake | Köster and Rahmann, 2012 | https://github.com/snakemake/snakemake |
| fastqc | Bioinformatics Group at the Babraham Institute | https://www.bioinformatics.babraham.ac.uk/projects/fastqc/ |
| multiqc | Ewels et al., 2016 | https://github.com/ewels/MultiQC |
| Trim-Galore! | Bioinformatics Group at the Babraham Institute | https://www.bioinformatics.babraham.ac.uk/projects/trim_galore/ |
| BBMAP | Bushnell, 2014 | https://sourceforge.net/projects/bbmap/ |
| GATK | DePristo et al., 2011 | https://github.com/broadinstitute/gatk |
| GenomicAlignments | Lawrence et al., 2013 | https://bioconductor.org/packages/GenomicAlignments |
| RSamtools | Morgan et al., 2020 | https://bioconductor.org/packages/Rsamtools |
| Rmarkdown | Xie et al., 2018 | https://github.com/rstudio/rmarkdown |
| UCSC genome browser | Kent et al., 2002 | http://genome.ucsc.edu |
| IGV browser | Robinson et al., 2011 | https://igv.org/ |
| Biostrings package | Pagès et al., 2020 | https://bioconductor.org/packages/Biostrings |
| Seurat package | Stuart et al., 2019 | https://github.com/satijalab/seurat |
| Other | | |
| Biosorter | Copas | N/A |
| Innova 42 programmable incubator | New Brunswick Scientific/Eppendorf | N/A |
| Precellys 24 tissue homogenizer | Bertin Instruments | N/A |
| nCounter | Nanostring | N/A |
| StepOnePlus real-time PCR system | Thermo Fisher | N/A |

## RESOURCE AVAILABILITY

### Lead contact

Further information and requests for resources and reagents should be directed to and will be fulfilled by the Lead Contact, Nikolaus Rajewsky (rajewsky@mdc-berlin.de).

### Materials availability

Plasmids generated for this work for heat-shock expression of Cas9 (pJJF152), sgRNA cloning (pJJF439) and proof-of-concept sgRNAs (SECGFP_sg1, SECGFP_sg2, dpy-10_CDS_sg1, sqt-3_UTR_sg2, dpy-10_CDS_sg6 in pJJR50 backbone, dpy-10_CDS_sg6 in pJJF439 backbone) have been deposited to Addgene (under IDs 163862, 164266, 163864, 163865, 163866, 163867, 164267, 164268). Plasmids for other sgRNAs (see Table S3) are available upon request.

*C. elegans* strains generated in this study (see Table S3) are available upon request.

### Data and code availability

The software "crispr-DART" created as part of this study is available at Github along with installation instructions and sample input files https://github.com/BIMSBbioinfo/crispr_DART.

The R scripts to reproduce the analyses and figures of this study are available at Github https://github.com/BIMSBbioinfo/froehlich_uyar_et_al_2020.

The accession number for the raw sequencing data reported in this paper is NCBI Bioproject: PRJNA701945.

The same raw sequencing data can additionally be found at the following link:
https://bimsbstatic.mdc-berlin.de/akalin/buyar/froehlich_uyar_et_al_2020/reads.tgz.

The sample sheet which describes the experimental setup for running crispr-DART can be found here:
https://bimsbstatic.mdc-berlin.de/akalin/buyar/froehlich_uyar_et_al_2020/sample_sheet.csv.

The output of crispr-DART for this data can be found here:
https://bimsbstatic.mdc-berlin.de/akalin/buyar/froehlich_uyar_et_al_2020/crispr_dart_pipeline_output.tgz.

The HTML report produced by crispr-DART for this study can be browsed here: https://bimsbstatic.mdc-berlin.de/akalin/buyar/froehlich_uyar_et_al_2020/reports/index.html.

## EXPERIMENTAL MODEL AND SUBJECT DETAILS

### *Caenorhabditis elegans*

The wild-type strain N2 Bristol (Fatt and Dougherty, 1963) was used to create transgenic lines for experiments. In a screen for phenotypes, we isolated several mutants and revertants for different regulatory regions. For initial tests we generated a *his-72* c-terminal GFP knock-in strain (NIK123) which we crossed into a strain expressing *Peft-3:tdTomato:H2B* from a single copy insertion (EG7927) (Frøkjær-Jensen et al., 2014) resulting in a GFP/tdTomato expressing strain (NIK124) for automated quantifications and sorting using the Copas Biosorter. A complete list of strains can be found in Table S3.

Animals were maintained on NGM plates with *Escherichia coli* OP50 as originally described (Brenner, 1974) at 16, 20 or 24°C. Plates for hygromycin resistant transgenic animals were modified by adding working stock solution of 5 mg/mL Hygromycin B (Thermo Fisher) in water onto plates before use, to a final concentration of 75 μg/mL NGM. For standard 6 cm plates with 10 mL NGM that would be 150 μL of 5 mg/mL Hygromycin working stock solution.

## METHOD DETAILS

### Plasmid construction

A list of all plasmids created or used in this study can be found in Table S3. The plasmid for heat-shock inducible *Streptococcus pyogenes* Cas9 expression (pJJF152) was created by Gibson assembly (Gibson et al., 2009) of a previously published *C. elegans* optimized SpCas9 (Friedland et al., 2013) ("Friedland Cas9"), with the *hsp-16.48* heat-shock promoter and the *unc-54* 3′ UTR using HiFi DNA Assembly Master Mix (NEB). The plasmid backbone for sgRNA expression (pJJF439) was created by PCR amplification of the U6 promoter of *W05B2.8* and replacing the promoter of pJJR50, using restriction digest and Gibson assembly.

Plasmids for sgRNA expression were cloned as previously described using one of two published backbones, pMB70 (Waaijers et al., 2013), pJJR50 (Waaijers et al., 2016) or pJJF439 (this study). For this, 5-10 μg of backbone was digested using 1 μL Fastdigest Eco31I (aka BsaI, Thermo Fisher) or Fastdigest BpiI (aka BbsI, Thermo Fisher) at 37°C for 2-6 hr, separated from undigested plasmid on a 1.5% Agarose/TAE gel, and extracted using the Zymoclean Gel DNA Recovery Kit (Zymo), according to the instruction manual. Two complementary DNA oligonucleotides containing the spacer sequence, plus an optional 5′ G for optimal U6 promoter expression, and 4 nucleotide overhangs for ligation into the backbone were phosphorylated and annealed in a thermocycler. This reaction contained 1 μL of each oligo (at 100 μM), 1 μL of 10x T4 DNA ligase buffer (Thermo Fisher), 1 μL T4 PNK (Thermo Fisher) and 6 μL water and was incubated 37°C 30 min, 95°C 5 minutes and cooled down at −0.1°C/second to 25°C. Sample was diluted 1:200 in water and 1 μL was used for ligation with 70-130 ng of linearized backbone, 1 μL of 10x T4 DNA ligase buffer and 1 μL of T4 DNA

ligase (Thermo Fisher) and water to a volume of 10 μL. Ligation was performed at room temperature for 1 hr or overnight. 5 μL were then transformed.

The HDR repair template plasmid used for the *his-72::GFP* knock-in was prepared as described previously (Dickinson et al., 2015).

For transformation and amplification, we used DH5alpha Mix & Go Competent Cells (Zymo) in all the above clonings except for the *his-72::GFP* repair template which required ccdB resistant bacteria for which we used One Shot ccdB Survival (Thermo Fisher). DNA extractions by miniprep were done with the ZymoPURE Plasmid Miniprep kit (Zymo) and elution with water.

### sgRNA design

Most sgRNAs were designed using the CRISPOR web application (http://crispor.tefor.net/) (Haeussler et al., 2016). Some sgRNAs were designed manually using the plasmid editor Ape (A plasmid Editor; M.W. Davis ; https://jorgensen.biology.utah.edu/wayned/ape/). All sgRNAs were designed for *C. elegans* genome version ce11 and we evaluated all sgRNAs using the E-CRISP web application (http://www.e-crisp.org/E-CRISP; Heigwer et al., 2014). For regulatory regions of interest, we aimed at a regular spacing between target sites, dense coverage and as little as possible predicted off-targets with less than three mismatches. A detailed list of sgRNA sequences, together with their characteristics, efficiency prediction scores and predicted off-targets can be found in Table S3.

### Generation of transgenic *C. elegans*

Simple extra-chromosomal array transgenes were generated by standard procedure using micro-injection into the gonad (Mello and Fire, 1995). A detailed list of injection mixes and their composition can be found in Table S3. The injection mix usually contained plasmids for heat-shock inducible Cas9, pMB67 (Waaijers et al., 2013) or pJJF152 (this study) at 50 ng/μL, 1-10 sgRNAs using the backbones pMB70 (Waaijers et al., 2013), pJJR50 (Waaijers et al., 2016) or pJJF439 (this study) at 10-50 ng/μL, a visual co-injection marker expressing mCherry in the pharynx, pCFJ90 (Frøkjaer-Jensen et al., 2008) at 5 ng/μL, and hygromycin resistance IR98 (Radman et al., 2013) at 3 ng/μL. For large scale experiments followed by targeted DNA sequencing we used pMB67 for Cas9 expression and sgRNAs cloned into the pJJR50 backbone. Independent lines were created from F1 animals selected for pharynx expression of the mCherry co-injection marker. Lines were maintained on Hygromycin selection plates as described above.

### C-terminal GFP knock-in of *his-72*

C-terminal GFP knock-in of *his-72* was performed as described previously using a self-excising selection cassette (Dickinson et al., 2015).

### Biosorter

Automated measurement of GFP negative animals in F1 and their F2 progeny. *His-72::GFP* was targeted with sg1, sg2, pool1 (sg2, 3, 4, 6, 8) or pool2 (sg3, 5, 8). F1 generation was collected by bleaching 12 hr after heat-shock. These were either measured on the Biosorter flow system at larvae stage L3 or grown to adulthood to collect F2 generation which was then also measured at larvae stage L3. The number of analyzed worms per sample was between 1,662 and 21,983 worms.

### Small-scale Cas9 induction and time course

20-40 egg-laying adults were transferred to small 6cm NGM plates with OP50 *Escherichia coli* and without Hygromycin. Plates were placed in a programmable incubator "Innova 42" (New Brunswick Scientific/Eppendorf) at 20°C. Heat shock was applied for 2 hours at 34°C, followed by 20°C. For time course experiments adults were transferred to new plates using a picking tool at regular time intervals (14, 16, 18, 20, 22, 43 or 12, 15, 18, 21, 48 hr) after heat shock to analyze eggs laid within each interval.

### Developmental synchronization

Synchronized L1s were obtained by bleaching, as previously described (Sulston and Hodgkin, 1988). Egg-laying animals were washed off plates in 50 mL M9 buffer (42 mM $Na_2HPO_4$, 22 mM $KH_2PO_4$, 86 mM NaCl, 1 mM $MgSO_4$) and settled for 10 minutes. M9 was aspirated until a remaining volume of 7.5 mL. Then 1 mL 12% NaClO and 1 mL 5 M NaOH were added. Worms were incubated under gentle rotation, vortexed briefly after 4 minutes and incubated under constant observation for another 3 minutes. Bleaching was stopped by addition of 40 mL M9 when circa 50% of animals were dissolved. Eggs were then pelleted by centrifugation at 1,200 g for 1.5 minutes and washed two more times using M9, centrifugation and decanting. Finally, eggs were resuspended in circa 4 mL M9 and left shaking at 16°C overnight for at least 12 hours to allow hatching and developmental arrest of L1 larvae. Larvae concentration was then counted in triplicates and the desired amount was dispensed on plates with food to begin synchronized development.

### Large-scale Cas9 heat shock induction

Before the experiments, animals were maintained 5-25 generations in culture under Hygromycin selection to ensure expression of transgenes. Expression was indicated by Hygromycin resistance and the visual mCherry co-injection marker expressed in the pharynx. For all experiments three independent lines from the same injection mix were used. For transient heat shock induction of Cas9, synchronized populations were seeded on large 15 cm NGM plates with food and without Hygromycin. Plates with egg-laying adults

(P0) were placed in a programmable incubator "Innova 42" (New Brunswick Scientific/Eppendorf) at 20°C and 34°C heat shock was applied for 2 hours. Plates were kept at 20°C for 12 hr and eggs were collected by bleaching as described above for developmental synchronization. Hatched larvae, arrested at the L1-stage, the first generation after Cas9 induction (F1), were then again seeded on large NGM plates with food for synchronized development until egg-laying, to collect the next generation (F2) by bleaching. We used this F2 generation for all experiments to ensure non-mosaic animals generated by F1 germline mutations. We seeded 50,000 P0 for Cas9 induction at 24°C on Hygromycin (25,000 / big plate), and 100,000 F1 at 16°C (25,000 / big plate). 400,000 F2 were frozen for genomic DNA extraction to determine introduced indel mutations. The remaining F2 were used for experiments described below.

### Genomic DNA extraction

Genomic DNA was obtained using worm lysis, phenol-chloroform extraction and ethanol precipitation. Worms were washed once in 50 mL M9 buffer and frozen in 1 mL M9. After thawing, M9 was removed and 100 μL of TENSK buffer (50mM Tris pH 7.5, 10 mM EDTA, 100 mM NaCl, 0.5% SDS. 0.1 mg/mL proteinase K, 0.5% β-Mercaptoethanol) was added. Sample was incubated for 1.5 hr at 60°C while shaking at 1,000 rpm on a benchtop heating block. 300 μL of water was added, followed by 400 μL phenol/chloroform/isoamylacohol pH 8.0 (Carl Roth). Sample was mixed by shaking the tube and centrifuged for 10 min. at 15'000 g at room temperature. The upper aqueous phase, circa 350 μL, was transferred to a new tube and an equal volume of chloroform was added. After additional centrifugation 10 min. at 15,000 g at 4°C, the upper aqueous phase was transferred to a new tube, and 2 μL glyco blue added. This was followed by addition of 30 μL 3M NaAc (pH 5.2-6) and 1 mL pure ethanol. Samples were centrifuged for 10 min. at full speed and 4°C in benchtop centrifuge. Pellet was washed once with 70% ethanol and resuspended in 25 μL water at 50°C for 30 min. Then 0.25 μL RNase I (10 U/μL, Thermo Fisher) was added and incubated for 30 min. at 37°C. DNA concentration was determined on a Nanodrop ND-1000 (Thermo Fisher) and diluted to 50-200 ng/μL in water.

### DNA long amplicon sequencing

Amplicons were designed so that they contained all the regions of a gene targeted in our experiments. 0.5 – 3 kb amplicons were large enough that deletions between the outermost sgRNAs would not change the amplicon size by more than 10% to avoid more efficient amplification of templates with large deletions. Furthermore, large amplicons should capture the reported large deletions missed by 100-300 bp amplicons of other workflows. Primers used for amplification together with annealing temperature and resulting amplicon sizes can be found in Table S3. Genomic DNA concentration was fluorimetrically quantified using Qubit dsDNA HS kit (Thermo Fisher). For PCR reactions we used 100 ng template DNA. We calculated that 100 ng of genomic DNA equals more than 90 million *C. elegans* genomes and therefore represented all animals in our samples that contained for most samples 400,000 and maximal (for DNA sampling over generations) 2,000,000 animals.

50 μL PCR the reactions were set up as follows. Phusion HF polymerase (NEB) 0.2 μL, 5X HF buffer 10 μL, dNTP mix 1 μL, forward and reverse oligos at 10 μM 5 μL, water 32 μL, and template DNA. Samples were incubated at 98°C 3 min, followed by 35 cycles of 98°C 15 s, 58-72°C 30 s, 72°C for 7 min with a final elongation at 72°C for 7 min. PCR reactions were analyzed on agarose gels to ensure successful amplification.

Cleanup was then done by either agarose gel or SPRI beads. For gel-based cleanup 1.5 % Agarose/TAE gels were run and bands were excised with circa ± 500 bp, to also include products with deletions or insertions. DNA was recovered from agarose gel using the Zymoclean Gel DNA Recovery Kit (Zymo). For SPRI beads cleanup and no size selection we used AMPure XP Reagent (Beckman Coulter). 0.8 x volume of beads were added to PCR reactions, incubated 2 min at room temperature, washed twice with freshly prepared 80 % EtOH using a magnetic rack, and eluted with water.

DNA was quantified by Nanodrop, diluted to 5 ng/μL, quantified by Qubit, diluted to 0.4 ng/μL, quantified by Qubit and diluted to 0.2 ng/μL for library preparation. Library preparation was done with the Nextera XT DNA kit (Illumina) which fragments input DNA and adds sample-specific barcodes by tagmentation. Although we used one barcode per sample, it is also possible to pool amplicons before library preparation and use the same barcode for multiple samples provided that samples don't need to be identified individually or that reads for each sample can be distinguished after mapping (e.g., non-overlapping amplicons from different genes). Libraries were analyzed with a Tapestation D1000 ScreenTape system (Agilent) or Bioanalyzer HS DNA kit (Agilent), and showed an average fragment size of around 500 bp (range 400 – 600 bp). Average fragment size, together with the DNA concentration measured with Qubit, was used to determine molarity and an equimolar pool of libraries was prepared. This pool was again analyzed using Tapestation or Bioanalyzer, measured by Qubit and diluted to 2 nM as input for the Illumina sequencing workflow. The library pool was then sequenced using 150 bp reads with a Miniseq Mid Output kit, 2x150 cycles (Illumina), or a Nextseq 500 V2 Mid Output kit, 150 cycles (Illumina).

### The crispr-DART software

In order to evaluate the outcomes of the CRISPR-Cas9 induced mutations by the protocol described in this study, we developed a computational pipeline to process the high-throughput sequencing reads coming from samples treated/untreated with CRISPR-Cas9. We made crispr-DART as generic as possible to accommodate different experimental setups, hoping that the pipeline can be useful to the scientific community carrying out genome editing experiments using CRISPR-based technologies, in particular those that aim to introduce many combinations of mutations in a genome via inducing double-stranded DNA breaks repaired by end joining

pathways. The pipeline can handle both short (e.g., single- or paired-end Illumina) but also long reads (e.g., PacBio). Each sample can contain multiple sgRNAs targeting multiple regions of the genome.

The first purpose of the pipeline is to serve as a quality control/reporting tool to evaluate the genome-editing experiment and address the following questions: Has the CRISPR-Cas9 treatment induced any mutations? If so, how are they distributed in the genome? Do the mutations that are commonly found in many reads originate at the intended cut site based on the designed guide RNA matching sites in the genome? How efficient were different guide designs in inducing DNA damage? Can we capture long deletions if there are multiple sgRNAs used in the same sample targeting nearby sites? How diverse are the deletions or insertions detected at the cut sites? We developed the pipeline to produce HTML reports collated into a website with interactive figures that help the user to quickly visualize and evaluate the outcomes of their experiment.

The second purpose of the pipeline is to produce many processed files containing information that can be useful for further analysis by external tools. Therefore, the pipeline's output consists of BAM files, bigwig files, BED files, and many different tables containing information about insertions and deletions along with the reads in which they were detected. In this study, many of the figures made for the manuscript were generated based on these intermediate files to address the many custom questions.

### Steps of the crispr-DART software

crispr-DART is implemented using Snakemake (Köster and Rahmann, 2012) following the practices as implemented for the PiGx pipelines (Wurmus et al., 2018). The pipeline consists of the following sequence of processing steps (see also Figure S2E):

#### Input

The input consists of a settings file in yaml format, which contains configurations for the tools used in the pipeline. Moreover, it contains file paths for where the sequencing reads are located, the target genome sequence to be used for mapping the reads, the sample sheet file which contains the experimental design (in comma-separated file format), the file containing the genomic coordinates of the expected sgRNA cut sites (in BED file format), and a table (in tab-separated format) that is needed for when a pair of samples are to be compared (for instance to observe the differences in per-base distribution of deletions detected in a treated sample and an untreated control sample, or to find specific deletions or insertions that are overrepresented in a sample compared to a control sample).

#### Pre-processing reads

Quality control using fastqc (https://www.bioinformatics.babraham.ac.uk/projects/fastqc/) and multiqc (Ewels et al., 2016) and quality improvement of reads using Trim-Galore! (https://www.bioinformatics.babraham.ac.uk/projects/trim_galore/).

#### Mapping and re-alignment

Mapping/alignment of the reads to the genome using BBMAP (Bushnell, 2014). We use BBMAP for read alignment because it can handle both long and short reads, both single-end and paired-end reads, both DNA and RNA reads, and it can help detect both short and long insertion and deletion events.

Re-alignment of reads with indels using GATK (DePristo et al., 2011). This step helps reconcile different indel alignments to minimize the noise in alignments.

#### Extraction of indels

Extraction of indels from the BAM files using R packages GenomicAlignments (Lawrence et al., 2013) and RSamtools (Morgan et al., 2020), producing the following output.

#### Output files

BED files: genomic coordinates of insertions and deletions.

Bigwig files: alignment coverage (how many reads aligned per each base of the genome).

Bigwig files: insertion/deletion/indel scores which represent the ratio of reads with an insertion, deletion or either (indel) to the number of reads aligned at a given base position of the genome. These files are very useful in visualizing profiles of the degree of mutations per-base resolution.

Tab-separated format files for the following:

Inserted sequences - this table contains the list of all reads with an insertion, along with the exact genomic coordinate of where the insertion occurs, and the actual sequence of the inserted segment.

Indels - This table contains the genomic coordinates of the deletions and insertions supported by at least one read along with how many reads support the insertions/deletions and the maximum depth of coverage (considering all reads) along the deleted segment or at the insertion site.

Reads with indels - This table is the complete list of reads with insertions/deletions along with the coordinates of the insertions/deletions.

sgRNA efficiency - This table contains statistics about the efficiency of each guide RNA in inducing mutations at the targeted site of the genome. The efficiency of a sgRNA is defined as the ratio of the number of reads with an insertion/deletion that start or end at ± 5bp of the intended cut-site to the total number of reads aligned at this region.

#### HTML reports

All the pre-processed files from the previous steps are combined to generate interactive (where applicable) HTML reports from all the analyzed samples that exist in the input sample sheet. For each targeted region (assuming a region of a few thousand base pairs that is sequenced), currently four different reporting Rmarkdown scripts are run. The resulting HTML files are organized into a website

using the 'render_site' function of the Rmarkdown package (Xie et al., 2018). Thus, all the processed data and outcomes can be quickly browsed through a website.

### Browser shots

Browser shots were compiled using indel profiles and top indels provided by the computational pipeline crispr-DART as BigWig and BED files and loading them into the UCSC genome browser (Kent et al., 2002) or the IGV browser (Robinson et al., 2011) followed by export as vector graphics compatible format. We used *C. elegans* genome version ce11/WBcel235 including 26 species base-wise conservation (PhyloP).

### sgRNA efficiency comparisons

Crispr-DART calculates the efficiency of a sgRNA as the ratio of the number of reads with an insertion/deletion that start or end at ± 5bp of the intended cut-site to the total number of reads aligned at this region. For untreated wild-type control samples, we used all cut sites present in any of the treated samples of the same amplicon. For comparing observed efficiencies to published prediction scores and other sgRNA characteristics, these scores were manually extracted from the CRISPOR web application (http://crispor.tefor.net/; Haeussler et al., 2016) for each sgRNA and compared to the sgRNA efficiencies determined by crispr-DART.

### Indel characteristics

For indel proportions, the fraction of reads containing insertion, deletion or complex events was determined per sample. Complex events were defined as reads containing more than one event. These could be either insertions, deletions or additional substitutions which suggested a combination of multiple events.

For the distribution of indel lengths we considered all deletions or insertions supported by at least 0.001% of reads at that position, at least 5 reads and overlapping with any cut site ± 5 bp. Deletions were further classified as "multi cut" deletions when a deletion overlapped with more than one sgRNA cut site ± 5 bp or otherwise were classified as "single cut" deletions when they only overlapped with one cut site (see also Figure S3B for a scheme describing this).

For the analysis of insertion origin, all 5-mers from insertions were extracted. Then matches to the surrounding sequence ± 50 bp of the insertion position were counted on the forward and reverse complement strand. As control sequences nucleotides of insertions were shuffled randomly.

R scripts to reproduce these analyses and figures are available at the Github repository (see Data and Code Availability section).

### Genotype diversity

For genotype diversity we considered indels supported by at least 0.001% of reads at that position, at least 5 reads and overlapping with any cut site ± 5 bp. Each deletion, defined by start and end coordinates, irrespective of its abundance (except reaching the threshold defined above) was considered as one unique deletion genotype. Each insertion genotype was defined by position and by taking into account the inserted sequence. For untreated wild-type control samples, we used all cut sites present in any of the treated samples of the same amplicon.

For the plots of "unique deletions per nucleotide by sgRNA," each deletion was assigned to a sgRNA when it was overlapping with its cut site ± 5 bp.

R scripts to reproduce these analyses and figures are available at the Github repository (see Data and Code Availability section).

### Targeted mRNA sequencing, *lin-41*

Mutated F2, arrested at the L1 developmental stage, were obtained from Cas9-induced P0 as described above. 40,000 were directly frozen for genomic DNA extraction. 80,000 were directly frozen for RNA extraction by adding 1 mL TRIzol reagent (Thermo Fisher), homogenization with a Precellys 24 tissue homogenizer (Bertin Instruments) and storage at −80°C. 5,000 L1s were seeded on large 15 cm NGM plates at 24°C and collected 32 hours later, at late-L4 stage, and prepared for RNA extraction like the L1 sample. At 32 hours, *lin-41* mRNA is fully downregulated (Aeschimann et al., 2017), while the lethal vulva bursting occurs later, after molting, in the adult stage (Ecsedi et al., 2015).

RNA was chloroform-extracted as follows. Samples were thawed, 0.2 mL of chloroform added, incubated for 3 minutes, and centrifuged for 15 minutes at 12,000 x g at 4°C. The upper aqueous phase was transferred to a new tube, 2 μL GlycoBlue (30 μg) were added, 500 μL of isopropanol were added and sample was incubated for 10 minutes. Sample was centrifuged 10 minutes at 12,000 x g at 4°C, supernatant discarded, and 1 mL of 75% EtOH was added. Sample was centrifuged for 5 minutes at 7,500 x g at 4°C, supernatant removed, pellet air-dried and resuspended in 20 μL RNase-free water. RNA concentrations ranged between 1,000 - 2,000 ng/μL, as determined on a Nanodrop ND-1000. Sample was diluted to 300 ng/μL and used for reverse transcription.

RNA was reverse transcribed using Maxima H Minus Reverse Transcriptase (Thermo Fisher). A reaction containing 11.5 μL RNA (3.45 μg), 2 μL gene-specific RT primer at 10 μM (oJJF890 "3′end," containing a UMI and PCR handle), 1 μL dNTP Mix (10 mM each), was incubated 5 minutes at 65°C. Then 4 μL 5X RT buffer, 0.5 μL RiboLock RNase inhibitor, and 1 μL (200 U) Maxima H Minus reverse transcriptase were added and the reaction was incubated for 30 minutes at 60°C, and 5 minutes at 85°C.

PCR was performed with a *lin-41*-specific primer containing a sample-specific barcode (oJJF1140-1147 for samples N2, 1516, 2627, pool3 at L1 and L4 stages) binding in the second last exon and a primer (oJJF960) binding the PCR handle introduced by

the reverse transcription primer. 2 μL of each RT reaction was used as template in 4 PCR reactions, each containing 10 μL 5X HF buffer, 1 μL dNTP mix (10 mM each), 5 μL F+R primer mix (10 μM), 0.2 μL Phusion polymerase, 32 μL water and 2.5 μL DMSO (5% final). Samples were incubated at 98°C 3 min, followed by 35 cycles of 98°C 10 s, 69°C 20 s, 72°C for 1 min with a final elongation at 72°C for 7 min. PCR was then analyzed on an agarose gel and DNA was cleaned up using Ampure XP beads (Beckman Coulter). For this the four PCR reactions were pooled resulting in 100 μL. 80 μL beads were added, incubated for 5 min at room temperature, washed once with 70% ethanol, and DNA was eluted in 10 μL water. This resulted in concentrations between 40-110 ng/μL. All samples were diluted to 40ng/μL and then pooled. 32 μL of this pool (1280 ng) was then used as the input for SMRTBell (Pacbio) library preparation according to the instruction manual and sequenced using a Pacbio Sequel I sequencer.

### RNA analysis of *lin-41* 3′ UTR deletions

Deletions supported by at least 5 Pacbio reads from L1 and L4 stage samples were filtered to keep only those deletions detected in both samples. No read percentage threshold was applied in this analysis. Each deletion was categorized based on their overlap with important sites in the 3′ UTR of *lin-41*.

- Seed region of the first *let-7* microRNA complementary site (site1) (“LCS1_seed”): chrI:9335255-9335263
- Seed region of the second *let-7* microRNA complementary site (site2) (“LCS2_seed”): chrI:9335208-9335214
- Non-seed nucleotides of the first *let-7* microRNA complementary site (site1) (“LCS1_3compl”): chrI:9335264-9335276
- Non-seed nucleotides of the second *let-7* microRNA complementary site (site2) (“LCS2_3compl”): chrI:9335215-9335227

Deletions were further categorized based on whether they overlap both *let-7* microRNA seed regions (“both”), and those that don’t overlap any of these defined regions (“none”).

Deletion frequency values were computed and the ratio of deletion frequencies between L4 stage and L1 stage samples were computed in log2 scale. For each category of deletions, a one-sided Wilcoxon rank-sum test was computed to test the null hypothesis that the stage specific abundance of deletions that overlap a *let-7* binding site is not greater from those deletions that don’t overlap any of these sites.

### RNA analysis by unsupervised clustering of long reads

Only Pacbio reads from both L1 and L4 stage *lin-41* RNA samples that covered the complete region between chrI:9334840-9336100 (the region from the beginning of the amplified segment up to the first intron) were selected, to make sure that all reads that go into analysis are covering the whole segment. For each read, the alignment of the read (including the inserted sequences) was obtained and all combinations of k-mers (k = 5) were counted within these alignments allowing for up to 1 mismatch using Biostrings package (Pagès et al., 2020). Seurat package (Stuart et al., 2019) was used to process the k-mer count matrix to do scaling, dimension reduction (PCA and UMAP) and network-based spectral clustering. The clustering of long PacBio reads covering the region enabled us to cluster reads into genotypes, thus taking advantage of the length of the reads while also allowing for the high rate of indels in the PacBio reads (compared to Illumina reads).

### DNA sampling over generations, *lin-41*

Mutated F1 samples were obtained as described above using large-scale mutagenesis by Cas9 heat shock induction. For this we used N2 as control and 3 lines with sgRNAs against the *lin-41* 3′ UTR (sg15 and sg16, sg26 and sg27, sg pool). We conducted the experiment at 16°C and 24°C. 3,000 L1 stage animals (F1 generation) were seeded on medium plates with OP50. After egg laying and hatching of the next generation (F2) after 3 or 5 days (24°C or 16°C) F1 and F2 were separated. For this, animals were washed from plates in a final volume of 2 mL M9 buffer into 2 mL Eppendorf tubes. Adult animals sink faster and after circa 2-5 minutes are collected at the bottom of the tube, while L1 animals still swim. This was carefully monitored visually. When most adults (95%) had sunken to the bottom, supernatant M9, containing L1 stage animals, was removed to a separate tube. This was repeated three times by adding 2 mL M9 and separation by sinking. Adult animals were frozen for genomic DNA extraction in circa 20 uL M9. For generations F2-F4, 2,000 L1 were seeded on new medium plates, and frozen as adults after separation from the next generation. Generation F5 was frozen at L1 stage. Genomic DNA extraction and targeted large amplicon sequencing was performed as described above.

### Fitness analysis of *lin-41* 3′ UTR deletions

For this analysis, we used *lin-41* DNA samples sequenced with Illumina single-end sequencing from multiple generations from F1 to F5 of the same pool of animals treated with sgRNA guides “sg15 and sg16,” “sg26 and sg27” or “sg pool.” Deletions were considered for this analysis when they were supported in the F1 samples by at least 0.001% of reads at that position and at least 5 reads. The important sites considered for this analysis were the following.

- Seed region of the first *let-7* microRNA complementary site (site1) (“LCS1_seed”): chrI:9335255-9335263
- Seed region of the second *let-7* microRNA complementary site (site2) (“LCS2_seed”): chrI:9335208-9335214
- Non-seed nucleotides of the first *let-7* microRNA complementary site (site1) (“LCS1_3compl”): chrI:9335264-9335276

- Non-seed nucleotides of the second *let-7* microRNA complementary site (site2) (“LCS2_3compl”): chrI:9335215-9335227
- Poly-adenylation signal: chrI:9334816-9334821
- Stop-codon: chrI:9335965-9335967

We wanted to address the question whether the deletions that exist at F1 were exposed to purifying selection over generations if they overlapped the important sites in the 3′ UTR region of *lin-41*. We did this analysis in two ways. First, we counted the deletions categorized by their overlap (or non-overlap) with the important sites that existed in F1 generation and analyzed how many of them still existed in later generations. Second, we did the same analysis at the level of reads: we counted the reads with deletions that overlapped or did not overlap the important sites from generations F1 to F5. When comparing the number of reads, the read counts were normalized by the library sizes (total number of reads in the sample).

### *Lin-41* strains with site1 or site2 deletions

We generated mutant strains by targeting either site1 or site2 using Cas9/tracRNA/crRNA RNP injections. Injection mix contained 0.3 μg/μl Cas9 protein (Alt-R Cas9 V3 from IDT), 0.12 M KCl, 8 nM HEPES pH 7.4, 8 μM tracrRNA (Alt-R from IDT), 8 μM crRNA (custom crRNA, Alt-R from IDT), 5 ng/μl pCFJ90 (RFP co-injection marker), in duplex buffer (IDT). To prepare injection mixes, Cas9 protein was mixed with KCl and HEPES. crRNA and tracrRNA were annealed in duplex buffer for 5 min at 95°C and ramp down to 25°C and added. Cas9/tracRNA/crRNA mix was incubated at 37°C for 10 min. F1 progeny positive for the pharynx expressed RFP co-injection marker were singled, allowed to lay eggs at 16°C, then genotyped using single worm lysis followed by Sanger sequencing of PCR amplicons. We observed mutations in 12/24 (50%) (site1) and 15/32 (47%) (site2) genotyped animals. For each site we kept the two strains with the biggest disruption of the seed regions. We maintained these strains at 16°C. Strains were bleached for developmental synchronization as described above. Three 10cm plates with egg-laying adults were bleached for each strain. For the strain MT7626 *let-7(n2853),* which shows developmental defects, six plates were bleached. L1 larvae hatched overnight at 16°C.

For RNA quantifications, 7000 L1 larvae were seeded onto medium 10cm plates and cultured at 24°C. 30 hours into synchronized development animals were collected using M9. After settling 200 uL were added to 1 mL of TRIzol reagent, homogenized in a Precellys 24 tissue homogenizer (Bertin Instruments) and stored at −80°C. Samples were thawed and RNA was chloroform-extracted as follows. 0.2 mL of chloroform were added, incubated for 3 minutes, and centrifuged for 15 minutes at 12,000 x g at 4°C. The upper aqueous phase was transferred to a new tube, 2 μL GlycoBlue (30 μg) were added, 500 μL of isopropanol were added and sample was incubated for 10 minutes. Sample was centrifuged 10 minutes at 12,000 x g at 4°C, supernatant discarded, and 1 mL of 75% EtOH was added. Sample was centrifuged for 5 minutes at 7,500 x g at 4°C, supernatant removed, pellet air-dried and resuspended in 20 μL RNase-free water. RNA concentrations ranged between 1,000 - 4,000 ng/μL, as determined on a Nanodrop ND-1000. Sample was diluted to 150 ng/μL and used for reverse transcription. RNA was reverse transcribed using Maxima H Minus Reverse Transcriptase (Thermo Fisher). A reaction containing 10 μL RNA (1. 5 μg), 2.5 μL water, 1 μL of random hexamer primer at 5 ng/μL, 1 μL dNTP Mix (10 mM each), was incubated 5 minutes at 65°C. Then 4 μL 5X RT buffer, 0.5 μL RiboLock RNase inhibitor, and 1 μL (200 U) Maxima H Minus reverse transcriptase were added and the reaction was incubated for 30 minutes at 60°C, and 5 minutes at 85°C. Quantitative real-time PCR (qPCR) was then performed using 10 μL SYBR green 2x (with 35 μL ROX/ 1mL), 2 μL forward and reverse primer mix (5 μM each), and 8 μL cDNA (10 ng/μL) (80ng total). Primers were tested using a stepwise four-fold dilution series for efficiency and melting curves for specificity. Reactions were performed in technical triplicates, water and RT- reactions served as controls for contamination and genomic DNA amplifications respectively. Differences in RNA/cDNA input were normalized using the tubulin gene *tbb-2* and fold changes were calculated relative to wild-type (N2) samples.

For quantification of phenotype, 200 L1 larvae were seeded onto small 6cm plates and cultured at 24°C. Photos and videos were taken at 50 hours into synchronized development. We then scored dead animals or animals that had burst (with the intestine exciting the body cavity through the vulva) by examining 200 animals per plate and 3 plates for each strain.

### Screen for regulatory sequences by phenotype

We targeted 8 genes with known RNAi-phenotypes (*dpy-2*, *dpy-10*, *egl-30*, *rol-6*, *sqt-2*, *sqt-3*, *unc-26*, *unc-54*) using different sets of sgRNAs against regulatory regions. We used lines in which we targeted the 3′ UTR and for some genes we used additional lines targeting predicted enhancer, TATA-box, initiator (INR) and upstream/promoter regions. A list with all samples can be found in Table S1.

For each transgenic line (injection mixes imJJF181-215) we screened 35,000 F2 animals produced from P0 with large-scale induced Cas9 expression as described above. Animals were seeded onto NGM plates with food at a concentration of 15,000 per 15 cm plates or at 2,500 - 5,000 per 10 cm plates. Plates were kept at 16°C or 24°C. We then directly screened these plates by eye. Additionally, we collected worms in M9 and dispensed worms in drops on an empty plate. We then observed worms moving in M9 and moving away after M9 was dried (< 1 min.). Dpy, Unc, and Rol worms were identified by morphology, their movement in M9 or slow and otherwise impaired movement away from the spot of dispension. Potential mutants were then picked and kept on plates for 2 to 4 generations at 24°C to achieve homozygosity. Animals were then singled again by phenotype and genotyped. This resulted in isolation of several mutant strains with the same genotype. We could not distinguish between cousins/siblings coming from the same F1/F2 or independent mutants coming from independently mutated F1s. In these cases, we kept one representative strain. We determined that penetrance was complete for all alleles except for the *sqt-2* enhancer locus (n > 300 animals). For

sqt-2 the penetrance varied between 10%–100%. We scored the expressivity of the phenotypes into three categories (+, ++, +++) (n > 300 animals). All the reported phenotypes have been determined and validated for several generations at 24°C. We also validated the absence of the extra-chromosomal transgenes judged by the red fluorescent co-injection marker. For *sqt-3* all isolated Dpy animals, characteristic for complete loss-of-function, contained large mutations affecting the coding frame. We therefore screened mainly for reduction-of-function alleles by screening for Rol animals. Non-Rol revertants of the *sqt-3(ins)* Rol animals were isolated using the small-scale approach on 6 cm plates (see above) with injection mixes imJJF215 or imJJF230.

### PCR Genotyping

Single worms were picked using a platin wire picking tool and immersed in 10 μL of worm lysis buffer (WLB) (10mM Tris pH 8.3, 2.5 mM $MgCl_2$, 50mM KCl, 0.45% NP-40, 0.45% Tween-20, 0.01% gelatine, and freshly added 100 μg/mL proteinase K). Samples were frozen at −80°C for at least 10 minutes, incubated at 60°C for 30-60 minutes, and 95°C for 15-30 minutes in a thermocycler. 1 μL of lysate was used as template in the following PCR. 25 μL PCR reactions were set up as follows. Phusion HF polymerase (NEB) 0.1 μL, 5X HF buffer 5 μL, dNTP mix 0.5 μL, forward and reverse oligos at 10 μM 2.5 μL, water 16 μL, and template DNA. 98°C 3 min, followed by 35 cycles of 98°C 15 s, 58-72°C 30 s, 72°C for 7 min with a final 7 min at 72°C. 2 μL of the reaction was then analyzed on an agarose gel. DNA was then cleaned up using AMPure XP Reagent (Beckman Coulter) by adding 0.8 x volume of beads to 23 μL PCR reaction, 2 min at room temperature, washed twice with freshly prepared 80 % EtOH using a magnetic rack, and eluted with 18 μL water. DNA was then either analyzed by T7 nuclease assay or directly sent to Sanger sequencing. T7 nuclease assay was performed on cleaned up DNA using T7 endonuclease. Sanger sequencing traces were aligned to genomic loci using Snapgene (GSL Biotech) and linear maps were exported as svg vector files to create figures.

### *Sqt-3* mRNA quantifications by Nanostring or qPCR

10 k L1-arrested synchronized animals were dispensed on 10 cm NGM plates with *Escherichia coli* OP50 at 24°C. Worms were then collected at different time points (22, 24, 26, 28, 30, 32 hr), washed once with M9 and homogenized in 1 mL of TRIzol reagent (Thermo Fisher) using a Precellys 24 tissue homogenizer (Bertin Instruments). RNA was isolated by standard phenol-chloroform extraction. RNA expression was quantified using an nCounter (Nanostring) which measures absolute RNA amounts using a set of gene-specific probes. Raw counts were normalized using reference genes (“house-keeping”). For quantitative real-time PCR (qPCR) of pre-mRNA and mRNA we used RNA from the 26 hr time point where *sqt-3* expression peaked. Pre-mRNA was specifically detected using intron-overlapping primers, while mRNA primers overlapped with exon-exon junctions. Controls without reverse transcriptase (“RT-“) were done to ensure specific amplification of cDNA and no amplification from potential contaminating genomic DNA. Final values were obtained by normalizing to pre-mRNA or mRNA of *tbb-2* and presented relative to N2 wild-type controls. QPCR was performed using Blue S’Green qPCR Kit following the instruction manual and quantification on a StepOnePlus real-time PCR system. Probes and primers can be found in Table S3.

### Transplantations into *dpy-10*, *unc-22* 3′ UTRs

Knock-in animals were produced using Cas9/tracRNA/crRNA RNP injections with ssDNA oligo repair templates. Injection mixes contained: 0.3 μg/μl Cas9 protein (Alt-R Cas9 V3 from IDT), 0.12 M KCl, 8 nM HEPES pH 7.4, 8 μM tracrRNA (Alt-R from IDT), 8 μM crRNA (custom crRNA, Alt-R from IDT), 3.15 ng/μl pJJF062 (GFP co-injection marker), 3.15 ng/μl pIR98 (HygroR), 0.75 μM of a ssDNA oligo repair template, in duplex buffer (IDT). To prepare injection mixes, Cas9 protein was mixed with KCl and HEPES. crRNA and tracrRNA were annealed in duplex buffer for 5 min at 95°C and ramp down to 25°C and added. Cas9/tracRNA/crRNA mix was incubated at 37°C for 10 min. Then plasmids and ssDNA repair template were added and 10 P0 animals were injected. For each injection mix 8 F1s positive for the co-injection marker were picked and genotyped using two PCR reactions (one primer pair flanking the insertion, the other with one primer binding in the insertion).

## QUANTIFICATION AND STATISTICAL ANALYSIS

The statistical parameters (i.e., exact values of n, what n represents, SEM, SD, confidence intervals, p values, mean, median etc.) and the performed statistical tests are reported in the Figure legends. No statistical methods were used to pre-determine sample size. The investigators were not blinded to allocation during experiments and outcome assessment.